AD

AD-E400 375

CONTRACTOR REPORT ALSCD-CR-79009

# RAPID ULTRASONIC INSPECTION OF ARTILLERY PROJECTILES

MURRAY W. MAHONEY, PROGRAM MANAGER
ROCKWELL INTERNATIONAL SCIENCE CENTER
THOUSAND OAKS, CA.

JOSEPH H. MULHERIN, PROJECT ENGINEER
ARRADCOM

NOVEMBER 1979


US ARMY ARMAMENT RESEARCH AND DEVELOPMENT COMMAND
FIRE CONTROL AND SMALL CALIBER
WEAPON SYSTEMS LABORATORY
DOVER, NEW JERSEY

UNCLASSIFIED

SECURITY CLASSIFICATION OF THIS PAGE *(When Data Entered)*

## REPORT DOCUMENTATION PAGE

READ INSTRUCTIONS BEFORE COMPLETING FORM

1. REPORT NUMBER: Contractor Report ARSCD-CR-79009
2. GOVT ACCESSION NO.:
3. RECIPIENT'S CATALOG NUMBER:

4. TITLE *(and Subtitle)*: RAPID ULTRASONIC INSPECTION OF ARTILLERY PROJECTILES

5. TYPE OF REPORT & PERIOD COVERED: FINAL - 09/29/78 thru 12/20/78

6. PERFORMING ORG. REPORT NUMBER: SC5186.24FR

7. AUTHOR(s): Murray W. Mahoney, Program Manager, Rockwell International Science Center
Joseph H. Mulherin, Project Engineer, ARRADCOM

8. CONTRACT OR GRANT NUMBER(s): DAAK10-78-C-0409

9. PERFORMING ORGANIZATION NAME AND ADDRESS:
Rockwell International Science Center
1049 Camino Dos Rios
Thousand Oaks, California 91360

10. PROGRAM ELEMENT, PROJECT, TASK AREA & WORK UNIT NUMBERS: Proj No. 5786654

11. CONTROLLING OFFICE NAME AND ADDRESS:
ARRADCOM, TSD
STINFO (DRDAR-TSS)
Dover, NJ 07801

12. REPORT DATE: November 1979

13. NUMBER OF PAGES: 46

14. MONITORING AGENCY NAME & ADDRESS*(if different from Controlling Office)*:
ARRADCOM, FC&SCWSL
Matls & Mfg Tech Div (DRDAR-SCM-P)
Dover, NJ 07801

15. SECURITY CLASS. *(of this report)*: UNCLASSIFIED

15a. DECLASSIFICATION/DOWNGRADING SCHEDULE:

16. DISTRIBUTION STATEMENT *(of this Report)*:
Approved for public release; distribution unlimited.

17. DISTRIBUTION STATEMENT *(of the abstract entered in Block 20, if different from Report)*:

18. SUPPLEMENTARY NOTES:

19. KEY WORDS *(Continue on reverse side if necessary and identify by block number)*:

Nondestructive testing
Electromagnetic acoustic transducers
Ultrasonics
Surface analysis
Carbon morphology
Artillery projectiles
Projectile inspection
Prototype
Metallurgy
Carbide morphology

20. ABSTRACT *(Continue on reverse side if necessary and identify by block number)*:

Results of a 3-month study to evaluate metallurgical and acoustic properties of HF-1 steel are presented. The objectives were to determine the cause of and solution for reduced ultrasonic signal generation efficiencies evident during ultrasonic inspection of M549 (RAP) artillery projectiles with electromagnetic acoustic transducers (EMATs).

It was shown that reduced generation efficiencies were the result of an in-process heat-treatment during fabrication and that the phenomenon was

DD FORM 1 JAN 73 1473 EDITION OF 1 NOV 65 IS OBSOLETE

UNCLASSIFIED

SECURITY CLASSIFICATION OF THIS PAGE *(When Data Entered)*

20. ABSTRACT (continued)

limited to the first ∿ 0.007 in. (0.178 mm) of surface material. Accordingly, surface material was examined prior to and following heat-treatment to determine the metallurgical and/or morphological changes that cause this impedence. A hypothesis is that reduced ultrasonic signal efficiencies are possibly the result of a weakly magnetic continuous grain boundary phase of $Fe_3C$. Some results are contradictory, however, and as such, studies should be continued to further evaluate this hypothesis.

In a normal magnetic bias, as opposed to a tangential bias, the surface condition of M549 (RAP) artillery projectiles had no effect on EMAT ultrasonic wave generation efficiencies. It was therefore recommended that the EMAT prototype inspection system for ultrasonic inspection of 155 mm M549 (RAP) artillery projectiles be designed with transducers located in a normal magnetic bias. This design change is considered minor and will have neither a significant financial impact on program performance nor influence the capability of the final product to perform reliably.

TABLE OF CONTENTS



LIST OF TABLES

LIST OF FIGURES

LIST OF FIGURES

## SUMMARY

This report presents results of a 3-month study to evaluate metallurgical and acoustic properties of HF-1 steel. The multiple objectives were to determine the cause and solution for reduced ultrasonic signal generation efficiencies evident during ultrasonic inspection of M549 (RAP) artillery projectiles with electromagnetic acoustic transducers (EMATs).

It was shown that reduced generation efficiencies were the result of an in-process heat-treatment during fabrication and that the phenomenon was limited to the first ~0.007 in. of surface material. Accordingly, surface material prior to and following heat-treatment was examined in an attempt to determine the metallurgical and/or morphological changes that impeded generation of ultrasonic waves with EMATs. Techniques used to characterize surface conditions before and after heat-treatment included chemical analysis, Auger spectroscopy, metallography, scanning electron fractography, transmission electron microscopy, x-ray measurement of residual stresses, strain gage measurement of magnetostriction properties and material acoustic response as a function of magnetic bias. In addition, similar evaluations were performed on other iron alloys containing varying levels of carbon. A compilation of results has led to the hypothesis that reduced ultrasonic signal efficiencies are possibly the result of a weakly magnetic continuous grain boundary phase of $Fe_3C$. Some results are contradictory, however, and as such, studies should be continued so that this hypothesis can be more completely evaluated.

It was also shown that in a normal magnetic bias, as opposed to a tangential bias, the surface condition of M549 (RAP) artillery projectiles had no effect on EMAT ultrasonic wave generation efficiencies. It was therefore recommended that the EMAT prototype inspection system for ultrasonic inspection of 155 mm M549 (RAP) artillery projectiles be designed and fabricated with transducers located in a normal magnetic bias. This design change is considered minor and will have neither a significant financial impact on program performance nor influence the capability of the final product to perform reliably.


## OBJECTIVES

The multiple objectives of this program are as follows:

1. Experimentally determine the reason for the signal launching failure in the ogive region of the Norris M549 projectile.

2. Evaluate appropriate corrective action to surmount this obstacle.

3. Qualitatively assess the capability of the corrective action to result in an EMAT ultrasonic inspection system that functions effectively and reliably in an artillery projectile metal parts production environment.

## INTRODUCTION

This report presents results for Sub-phase A of the third phase of a three phase program designed to evaluate the capability of using electromagnetic acoustic transducers (EMATs) for nondestructive inspection of M549 (RAP) artillery projectiles. In Phase I, EMAT inspection feasibility was demonstrated using the M107 projectile (ref. 1). Based on the successful results of Phase I, Phase II was used to develop specific components of hardware (ref. 2). Both of these previous phases have yielded promising results, details of which can be found in references 1 and 2. However, during Phase II, a surface phenomenon was observed in the ogive of the Norris Industries' M549 projectile that reduced EMAT efficiencies to unacceptable levels. Accordingly, Phase III of this program was divided into two sub-phases: Sub-phase A, the determination of the cause for reduced EMAT efficiencies in the ogive and an appropriate solution, and Sub-phase B, development, construction and evaluation of a prototype EMAT inspection system. Successful completion of Sub-phase A was required prior to initiation of Sub-phase B.

Although the purpose of this report is to present experimental results associated with this surface phenomenon, it is helpful to understand the principles of electromagnetic transduction necessary to excite ultrasonic waves with EMATs. Briefly, an EMAT transducer consists of a coil of wire carrying a dynamic current at the desired ultrasonic frequency, and a magnet to impress a static bias field. Ultrasonic waves are launched as a reaction to electromagnetic forces exerted when the transducer is placed adjacent to the surface of a metal part; they are detected by reciprocal processes. Since absolutely no physical contact is required, the transducers can be moved rapidly over a part without fear of disturbing the coupling medium. (For a detailed discussion of electromagnetic generation of ultrasonic waves, the reader is directed to References 2, 3 and 4.)

To maintain some continuity and to present this research in as complete a manner as possible, this document will discuss all research completed to date concerning this signal launching phenomenon. This will include results from 1) Sub-phase A of Phase-III, 2) Phase II, and 3) basic studies under the direction of Rockwell International IR&D program that add to an understanding of this phenomenon.

## EXPERIMENTAL EVALUATION OF ULTRASONIC SIGNAL LAUNCHING PHENOMENON

During Phase I, and throughout most of Phase II, M549 projectiles fabricated by Flinchbaugh were used to evaluate the feasibility of ultrasonic inspection using EMAT technology. Using these projectiles, ultrasonic signals were routinely launched from EMAT transducers and naturally occurring defects were readily located. During fabrication by Flinchbaugh, the projectiles had been machined on the OD surface and thus, any surface phenomena resulting from prior heat treatments or hot working operations would have been removed. At a later date, projectiles fabricated by Norris Industries in a 1975 lot were received by the Science Center for feasibility evaluation. No difficulties

were encountered in inspecting the body of the projectile, i.e., the area between the base and the location where the nose taper begins (bourrelet). This region is a machined surface, and again, any surface conditions affecting inspectibility would have been removed. On this same projectile, in regions exhibiting a hot worked surface (ogive), ultrasonic signal intensities were found to decrease by a factor of 15 (23 dB) as compared to corresponding locations on machined projectiles. However, after removal of a thin layer by machining, signal intensities were restored.

The following paragraphs of this section (1 through 5) present observations and results of experiments that both characterize this surface layer and evaluate the influence of this layer on electromagnetic generation of ultrasonic waves.

Ultrasonic Response

Figure 1 illustrates the difference in ultrasonic signal amplitude for different locations on a Norris M-549 (RAP) artillery projectile, i.e., the machined surface of the bourrelet, (fig. 1a), versus the hot worked surface of the ogive, (fig. 1b). These results are for a 400 Gauss tangential magnetic field, using one transducer for both transmitting and receiving an ultrasonic wave that completes one revolution. To avoid misinterpretation note the difference in scales between (figs. 1a and 1b). As can be seen for comparable parameters, inspection in the ogive results in an approximately 27 dB loss when compared to the bourrelet.

To illustrate that this signal amplitude loss is the result of a thin surface layer on the projectile, (fig. 2) shows received ultrasonic signal amplitudes vs depth of metal removed from the OD surface in the ogive region of an M549 (RAP) artillery projectile. It should be understood that due to eccentricity, metal removal is not uniform; this results in some uncertainty in the absolute magnitude of the data. However, it is clear that initial removal of material results in an immediate increase in signal amplitude, and that after approximately 0.007 in. (0.178 mm) of material is removed, signal amplitudes are comparable to those obtained in the bourrelet.

Influence of Processing Variables on Ultrasonic Efficiency

During fabrication of M549 (RAP) projectiles, a number of thermomechanical operations are employed that permanently alter the metallurgical condition of the final product. For example, hot worked steel products usually become somewhat decarburized during heating prior to a hot working operation. The depth and magnitude of decarburization depends on the hot working temperature, time at temperature, furnace atmosphere, reduction of area between the bloom and the finished size, and the type of steel. Considering the forming operations necessary to fabricate an M549 artillery projectile, e.g., nosing operations in air at 1525°F (829°C), it could be expected that the high carbon steel used for this fabrication (HF-1 steel with ~1.1% C) would exhibit some degree of surface decarburization. Similarly, heat treatments, metal removal

and metal forming operations are all processes that can result in both micro- and macro-residual stresses. Since previous work by R. B. Thompson (ref. 5) has shown that ultrasonic signal amplitudes are influenced by stress state, any of a number of processing steps used in the fabrication of projectiles could be creating the surface condition that manifests itself as reduced EMAT ultrasonic signal amplitudes.

In order to determine which fabrication step adversely influences ultrasonic inspection with EMATs, three M549 (RAP) projectiles were acquired from different locations on the Norris production line. Locations evaluated included 1) prior to hot nosing, 2) prior to final heat-treatment, and 3) following the final heat-treatment. Ultrasonic efficiency with EMATs was evaluated in the ogive region for each of these projectiles using a 400 Gauss tangential magnetic bias. Results shown in fig. 3 can be interpreted as follows:

- Figure 3a - Prior to the nosing operation, peak-to-peak signal amplitude measures ~8 volts and is equivalent to similar results obtained on projectiles fabricated by Flinchbaugh. Thus, up to this fabrication step EMAT ultrasonic signal efficiencies are not adversely affected.

- Figure 3b - Prior to heat-treatment (the nosing fabrication has now been completed), signal amplitude measures ~6.4 volts peak-to-peak. Interestingly, the metal reduction during nosing had little measurable influence on EMAT efficiency.

- Figure 3c - After heat-treatment, peak-to-peak signal amplitude is reduced to 0.24 volts. It can be concluded from these results that the heat-treatment alters material properties in such a manner that ultrasonic wave generation efficiency, using electromagnetic transducers, is severely reduced.

The effect of heat-treatment on EMAT signal efficiency is not limited to HF-1 steel. A 1090 tool steel has been shown to react similarly to heat-treatment (1525°F (829°C)/4 h WQ), whereas lower carbon steels such as 1018 and 1045 are relatively unaffected. Figure 4 illustrates these results and shows signal generation efficiency as a function of carbon content and heat-treatment for the above four steels. The implication from this work is that carbon distribution can be altered and result in a carbon morphology or microstructure that is not conducive to ultrasonic inspection with EMATs when inspection is performed in the magnetostrictive enhancement regime.

Characterization of Carbide Morphology

To qualitatively evaluate the influence of the furnace atmosphere during heat-treatment on the resultant ultrasonic efficiency of an M549 (RAP) projectile, a projectile was longitudinally sectioned such that each half contained both an inspectable surface (machined bourrelet) and a

noninspectable hot worked surface (ogive). One half of this projectile was decarburized by heat treating at 1525°F (829°C)/4 h, followed by an oil quench in air; the other half was carburized by heat treating at the same temperature in an endothermic base atmosphere with the dew point set to correspond to 1.1 points of carbon. After carburization, both surfaces were inspectable, whereas after decarburization, signal intensities were reduced for each surface condition. The sequence of operations corresponding to these results is shown in figure 5; figure 6 illustrates signal efficiency at the same location in the ogive for both a decarburized and carburized projectile. This experiment shows that not only could decarburization reduce signal levels, but inspectability of a decarburized surface could also be restored by heat treatments conducive to restoration of the original carbon level. Characterization of carbon morphology by chemical analysis, Auger spectroscopy, optical microscopy, and transmission electron microscopy (TEM) are discussed in the following sections.

Chemical Analysis

A carbon analysis through the thickness in the ogive of an M549 projectile is shown in figure 7. From this figure, it can be concluded that a carbon gradient does exist on both the ID and OD surfaces. However, the average carbon level remains relatively high. It should be realized that each of the data points in figure 7 represents an average carbon content for a given thickness, and as such, the carbon level on the extreme surface is not known. These results would support the hypothesis that if, indeed, the reduction in ultrasonic amplitude is associated with the carbon level, then it must be the chemisry in the first few mils. Figure 2 supports this contention, wherein the ultrasonic signal amplitude does increase after 0.001 in. (0.254 mm) of metal removal.

Auger Spectroscopy

Fracture specimens from M549 (RAP) projectiles, both before and after heat-treatment, were prepared for examination by Auger spectroscopy. Each specimen was 0.030 in. (0.762 mm) thick and preserved the OD surface while progressing 0.030 in. (0.762 mm) through the thickness. The possibility of contamination of fracture surfaces was prevented by fracturing each specimen inside the Auger vacuum chamber at $\sim 10^{-10}$ torr. Specimens were prepared in triplicate to evaluate repeatability of results. A carbon gradient, represented by a C/Fe ratio, was determined for each HF-1 steel specimen. (Figure 8 illustrates representative data for each material condition. It should be understood that the ordinant scale is dimensionless and that no absolute value of carbon or iron is to be implied by this figure.)

It is clear from this result that heat-treatment causes a large change in carbon distribution, i.e., within the first ~0.007 in. (0.178 mm) the quantity of carbon is decreased by an order of magnitude as a result of heat-treatment. At depths greater than ~0.007 in. (0.178 mm), carbon levels are relatively equivalent. Scanning electron fractographs, figure 9, illustrate a

corresponding change in fracture mode. Comparing figures 9a and 9b, shows the fracture mode changes from entirely ductile to a mixed mode of ductile fracture with regions of brittle faceted fracture.

Results shown in figure 8 are not completely understood. For example, the source for the high carbon level near the surface prior to heat-treatment is unknown. Also, after heat-treatment, this result shows the relative carbon level within the first 0.0003 in. from the OD surface is equivalent to the carbon level in the interior, while bulk chemistry results, figure 7, represented an average C level for the first 0.005 in. Apparently, the cause for reduced EMAT efficiencies is more than simply the quantity of C near the surface.

Optical Microscopy

Optical micrographs are shown in figure 10 for 1090 tool steel and figure 11 for HF-1 M549 (RAP) projectile steel. Microstructures are shown for material conditions prior to heat-treatment and after heat-treatment (4 h in air/1525°F WQ). Both materials, prior to heat-treatment (figures 10a and 11a), show a high density of $Fe_3C$ precipitates in a large grain ferrite matrix. After heat-treatment, the structure transforms to a very fine grained martensite with a slightly reduced density of $Fe_3C$ particles (figures 10b and 11b). Near the surface, the 1090 steel shows a grain boundary network of $Fe_3C$ (figure 10c) whereas the HF-1 steel, after heat-treatment, shows little difference between the surface and interior (figure 11c).

Each of the materials, prior to heat-treatment, were of such condition as to be readily inspectable with EMATs in a 300 Gauss tangential magnetic field. After heat-treatment, EMAT ultrasonic wave generation efficiencies were reduced in an equivalent manner to results illustrated in figure 6. The difference in microstructure prior to and following heat-treatment include: 1) the change in phase from ferrite to martensite and 2) the semicontinuous $Fe_3C$ phase throughout the grain boundaries near the surface in the 1090 steel (figure 10c). Ultrasonic waves are readily launched in martensite with EMATs, as illustrated by the increase in signal intensity as surface material is removed (figure 2). Thus, the phase change from ferrite to martensite is not the cause for reduced signal efficiencies.

Previous work (ref. 1) has shown that a pearlitic structure can reduce the efficiency of electromagnetic transducers. Pearlite results from the $Fe_3C$ eutectoid reaction involving the simultaneous formation of ferrite and carbide from austenite of eutectoid composition. Since the carbide and ferrite form simultaneously, they are intimately mixed. Characteristically, the mixture is lamellar, i.e., it is composed of alternate layers of ferrite and carbide. Neither the 1090 steel nor the HF-1 steel showed any evidence of pearlite. However, figure 10c does show the existence of a semicontinuous grain boundary network of $Fe_3C$. It was previously hypothesized (ref. 1) that reduced signal levels were caused both by the weak magnetic-properties of the $Fe_3C$ phase and by the lamellar structure of the pearlite. Although not as obvious, there is

some evidence to suggest the existence of a layered structure consisting of continuous or semicontinuous $Fe_3C$ at prior ferrite boundaries surrounding a fine martensite phase (figure 10c). It is possible that the presence of this weakly magnetic $Fe_3C$ grain boundary phase could be creating a morphology effectively equivalent to pearlite in its response to electromagnetic ultrasonic wave generation. This subject is discussed more completely in the next section, transmission electron microscopy.

Transmission Electron Microscopy

In the previous section it was hypothesized that the reduction in magnetostrictive enhancement of ultrasonic waves was possibly due to the redistribution of iron carbides that form either a continuous or semicontinuous weakly magnetic $Fe_3C$ grain boundary phase. Transmission electron microscopy (TEM) techniques were used to evaluate this hypotheses more completely.

Three steels, 1045, 1090, and HF-1, with known EMAT ultrasonic wave generation behavior for both the pre and post heat-treatment material conditions, were characterized as to carbide morphology. The EMAT ultrasonic efficiency of each of these materials before and after heat-treatment is illustrated in figure 4, i.e., prior to heat-treatment all three materials exhibited good magnetostrictive enhancement of ultrasonic waves, whereas after heat-treatment only the 1045 steel maintained a relatively high signal amplitude.

For the 1045 steel, figure 12 illustrates a complete absence of precipitated carbides or network of grain boundary carbides following heat-treatment. Again this material exhibits magnetostrictive enhancement of ultrasonic waves. Figure 13 illustrates results on 1090 steel both prior to and following heat-treatment. Prior to heat-treatment, figure 13a shows evidence of large precipitated carbides that have broken away from the specimen during foil preparation. There is no evidence of a continuous or semicontinuous grain boundary phase. However, after heat-treatment, figure 13b, carbide precipitates are smaller, display an increased density, and tend to align along prior ferrite grain boundaries. Material shown in figure 13a exhibits magnetostrictive enhancement, whereas material in figure 13b does not. TEM results on HF-1 material are shown in figure 14. Figures 14a and 14b illustrate carbide morphologies for material taken within 0.007 in. (0.178 mm) of the OD surface prior to and following heat-treatment. It is material properties within this surface layer that have adversely influenced EMAT ultrasonic signal amplitudes. Figure 14b illustrates a continuous grain boundary network of carbides as compared to the absence of a network of carbides prior to heat-treatment, figure 14a.

Clearly, the above results consistently support the proposed hypothesis. However, a possible anomaly exists when considering TEM results from a foil prepared some distance from the OD surface of an M549 projectile, figure 14c. In this figure a high density of carbides, including a semi-continuous grain boundary network, is evident. This material does maintain good magnetostrictive enhancement of EMAT ultrasonic waves, despite the observed semi-

continuous carbide morphology. If indeed grain boundary carbides are the source of reduced signal efficiencies, then there must be a subtle dividing line that distinguishes between semicontinuous and continuous carbides and also establishes EMAT ultrasonic efficiencies. It will be necessary to evaluate the proposed hypothesis in greater detail before it can be established as a proven conclusion.

Evaluation of Surface Residual Stresses

It has been demonstrated that the efficiency of the electromagnetic generation of ultrasonic waves in ferrous metals is strongly influenced by superimposed elastic strains (ref. 5). To determine if elastic strains are influencing signal generation efficiencies in M549 (RAP) projectiles, surface and indepth residual stress distributions were determined for different manufacturing conditions. Typically, manufacturing operations should impart stress distributions along the following rationale:

- Grinding: Abusive surface grinding is expected to produce tensile residual stress on the surface with considerable point-to-point variations. This is believed to be due primarily to nonuniform temperature distributions at the workpiece during the grinding process. Gentle grinding, which produces substantially lower heat generation in the workpiece, is known to impart compressive residual stresses due to cold work.

- Decarburizing: Distribution of the residual stress is determined by the carbon content and its effect on the $M_s$ temperature ($M_s$ decreases with C content) in relation to the temperature gradient as influenced by quench severity. Generally, decarburizing produces tensile surface stresses. Subsequent tempering severely decreases the magnitude.

- Carburizing: Same rationale as that for decarburizing, except that compressive residual stresses are expected. Also, large differences between hoop (tangential) and radial (longitudinal) stresses are normally found.

However, metallurgical factors such as C content and processing variables such as quench rate usually preclude an accurate estimate of the magnitude (and sometimes sign) of the surface residual stress. Residual stress measurements were therefore obtained at a number of locations, both as a function of depth from the surface and material condition, i.e, ground, hot-worked, carburized and decarburized surfaces. Results of these experiments are tabulated in Table 1 with typical data illustrated in figure 15. Radial stresses were measured on Samples A and B and, as seen in table 1, exhibit good isotropic characteristics. Thus, only hoop stresses were determined on the remaining samples. These measurements were conducted by EMS Laboratories, Hawthorne, CA, using a "Fastress" residual stress analyzer. This instrument is based on the two-tilt X-ray diffraction peak shift technique and averages

the lattice strain over an area of $2mm^2$ to a depth of ~20μm. An estimate of the absolute accuracy of the instrument and operator is ± 8 ksi with a relative precision between each measurement of ± 4 ksi.

Sample A, a ground surface with good EMAT ultrasonic wave generation efficiency shows a thin tensile surface stress which rapidly decays with depth. Sample B, a hot worked surface with poor transducer efficiency exhibits a strong and deep compressive zone (see figure 15). This stress condition would not be expected from a decarburized surface even after a subsequent tempering treatment. Obviously, the measurements do not indicate the usual pattern of residual stress typical of a decarburized surface. It would be safe to say that another effect, perhaps that of forging, is overriding the process. Similarly, samples E, G, and I all have similar compressive residual stress distributions and corresponding poor signal efficiencies. Interestingly, small cracks, which could be due to either the forging process or what is often termed "decarb cracking," were highly visible on sample G, which may indicate a tensile surface stress at some time in the processing.

The principle concern is with the ability to launch acoustic waves and the effect residual stress distributions may have on this launching. Results in table 1 demonstrate that there is no consistent correlation between signal efficiency and surface residual stresses. For example, as noted above, in Samples B, G, and I, acoustic waves cannot be launched, possibly because of the high compressive stress (ref. 5). In comparison, good transducer efficiency takes place in Sample A (tensile surface stress); however, good transducer efficiency is also obtained in samples C, D, and F, all of which contain highly compressive residual stresses. These results are not in accordance with the compressive stress hypothesis. Therein lies one anomaly. Second, removal of 0.007 in. (0.178 mm) from the surface of the ogive has been shown to increase the transducer efficiency to ~85% of that found in the bourrelet (figure 1). The stress measurements on Samples B, G, and I show the compressive layer to extend beyond 0.010 in. (0.254 mm) in depth. Third, the surface on carburized Sample D, a process that has been shown to restore signal efficiencies, retained compressive residual stresses even after the carburizing heat-treatment.

It is clear that residual stresses alone are not accountable for reduced wave generation efficiencies. It is worth noting, however, that a comparison of residual stress distributions before and after heat-treatment (Samples H and I), results in a large increase in compressive residual stresses on the surface. Thus, the possibility does exist for residual stresses to act in a synergistic manner with one or more other parameters to reduce EMAT ultrasonic wave generation efficiences.

Magnetic Field Dependence of EMAT Ultrasonic Wave Generation Efficiency

Prior work has shown the heat-treatment process at Norris Industries to be detrimental to generation efficiency of EMAT ultrasonic waves when using a tangential field. Accordingly, the EMAT ultrasonic wave generation efficiency

both prior to and following heat-treatment has been evaluated as a function of magnetic field bias. These results are shown in figures 16 and 17.

Figure 16 illustrates ultrasonic signal amplitude for an M549 (RAP) projectile with a tangential magnetic bias, i.e., EMATs located 90° from electromagnet pole pieces. As expected, prior to heat-treatment, magnetostrictive enhancement is observed as would be predicted with a ferromagnetic material. However, after heat-treatment, although ultrasonic waves are present in the material no magnetostrictive enhancement of signal amplitude is observed.

Conversely, in a normal magnetic bias, i.e., transducer located directly between the pole pieces and metal part being inspected, figure 17 shows that heat-treatment has no apparent effect on signal efficiency. For this transducer location there is no dependence on magnetostrictive enhancement for signal efficiency. From this result it becomes apparent that M549 (RAP) projectiles are readily inspectable with EMATs in a normal magnet bias and that difficulties in wave generation are uniquely associated with the tangential bias where magnetostrictive enhancement is necessary.

Efforts were made to measure magnetostrictive properties before and after heat-treatment for surface material within the first 0.007 in. (0.178 mm) and for material further through the wall thickness. Specimens representing these four conditions were appropriately strain gaged on each surface (to negate strains associated with bending stresses) and were coupled with dummy strain gages (to compensate for temperature fluctuations). It should be realized that this experiment was sensitive to the surrounding environment and was also dependent on uncontrolled external constraints, e.g., two specimens were <0.007 in. (0.178 mm) thick, magnetostrictive strains are very small, and the magnet was quite massive. Accordingly, an effort was made to perform experiments with a minimum time lag using identical procedures. Results for surface material and interior material before and after heat-treatment are illustrated in figures 18 and 19, respectively. In the region of interest for magnetostrictive enhancement of electromagnetic ultrasonic waves, 200 to 400 Gauss, the results are quite clear, i.e., there appears to be no effect of heat-treatment on magnetostrictive properties for either the surface or interior material.

Based on this result and the previously reported carbon morphology investigation, it is hypothesized that the cause for the lack of magnetostrictive enhancement is associated in some manner with the continuous grain boundary carbides and that magnetostrictive measurements are predominantly influenced by islands of martensite phase which comprise over 90% of the volume of the specimens.

## Recommendations

Based on the above results, efforts should be continued to more systematically evaluate carbon level and carbide morphology while evaluating corresponding effects on EMAT ultrasonic wave generation efficiency. These efforts

should include additional materials that also develop weakly magnetic grain boundary phases and should evaluate different steel microstructures. Future studies, however, should not be limited to the above. Many of the current results are contradictory, and it is entirely possible that the cause for reduced signal efficiencies has yet to be identified. In addition to the above, if necessary and if possible, the influence of carbon content, carbide morphology, and microstructure on material properties important to EMAT ultrasonic wave generation should also be determined, i.e., electrical conductivity, magnetic permeability and magnetostriction.

## PROPOSED CORRECTIVE ACTION

The above results have shown that in a normal magnetic bias, EMAT ultrasonic wave generation efficiencies are not influenced by the surface conditions associated with M549 (RAP) projectiles (figure 17). However, to perform ultrasonic inspection with this normal magnetic bias will require a design change such that transducers are now located between the pole pieces and the projectile, as opposed to the previous design where transducers were located 90° from the axis of the pole pieces. This design change will have little impact on the overal technical merit of this program or on similar follow-on programs. This conclusion is based on the following concerns which have been addressed prior to recommending this change:

Will additional design changes become necessary?

- It will now be necessary to design an automatic transducer tracking system that can be located in the gap between pole pieces and the projectile rather than on top of the projectile. A 0.25 in. (6.35 mm) gap exists between pole pieces and projectile and as such, the location of a fixture and transducers in the gap is not considered to be a major change.

- Power requirments to drive the electromagnet will increase. It will now be necessary to achieve an approximately 12 to 14K Gauss field in the gap, as opposed to the ~6K Gauss field present in the gap during inspection with a 300 Gauss tangential field. Since the electromagnet is operational for only a small fraction of the total inspection time, the increased energy consumption is considered insignificant.

Will previously constructed hardware and machine drawings still be applicable?

- The electromagnet pole pieces and coils may require redesign resulting in alteration or refabrication. The pole pieces will now be required to generate 12 to 14K Gauss in the air gap, and as such, modification of the existing pole pieces is now in progress in order to determine if sufficient magnetic field can be achieved with existing components. As noted above, power requirements have increased, thus, existing coils will be

required to carry additional current. It is possible that excessive heat may be generated; this would require forced air cooling of the coils or refabrication in order to reduce resistance heating. Neither of the considerations pose a major obstacle to program progress.

- Engineering drawings have been prepared for a walking beam metal parts transfer system and a handling machine station for lift and rotation of the projectile. Designs were such that these two units would be compatible. The program no longer includes the walking beam. However, the inspection station as designed can be upgraded to include the walking beam at a later date for an increase in funding. Also, due to increased magnetic forces, equipment designs have been reevaluated to accommodate the higher forces on the projectile handling apparatus. No large impact is expected.

Will capabilities to locate EDM notches, as prescribed per Army inspection requirements, be affected?

- Considering first the rate of inspection, there is no reason to believe that the speed of inspection will be influenced by the proposed design change.

- Figure 17 shows EMAT ultrasonic signal efficiencies in a normal magnetic field are equivalent prior to and after heat-treatment. Also, comparing figures 16 and 17, it is apparent that maximum signal efficiency due to magnetostrictive enhancement can be matched by inspection in a normal field at approximately 14K Gauss. Accordingly, capabilities to locate EDM notches, in a tangential and normal magnetic bias should be equivalent. To demonstrate capability to locate EDM notches, equal to and smaller in size than Army inspection requirements, EMAT ultrasonic signals resulting from reflection of ultrasonic waves from OD longitudinal notches are illustrated in figures 20b-i. The location of these notches is shown in figure 20a, with notch dimensions tabulated in table 2. These results were obtained with a 14K Gauss normal field using one EMAT transducer as both transmitter and receiver. Clearly, signal to noise ratios are more than satisfactory for determining both the existence of and location of standard EDM notches.

- The ability to locate ID notches in a normal magnetic bias has not as yet been confirmed. This is possibly due to the inability to establish a normal magnetic bias in the large electromagnet used for these experiments. That is, the magnetic field, because of the pole piece configuration and projectile geometry, is not necessarily normal to the projectile. It is anticipated that with the magnet specifically designed for the M549 (RAP) projectile this difficulty will be overcome.

What will be the financial impact of this design change on this program and subsequent construction of similar units?

- Based on the above discussions there will be little increase in materials cost. No additional funding will be necessary for successfull completion of design and construction of a prototype EMAT ultrasonic inspection station (Phase III-B).

- Future systems will not significantly increase in cost because of this design change, i.e., the increase in cost associated wtih normal field inspection will be <5% when compared to inspection in a tangential field.

Thus, based on demonstrated inspection capabilities and low financial impact, it is recommended that the EMAT prototype artillery projectile system be constructed with the intention of performing ultrasonic inspections in a normal magnetic field.

## CONCLUSIONS

- Experimental results have led to the hypothesis that reduced EMAT ultrasonic wave generation efficiencies in HF-1 and 1090 steel, under specific metallurgical conditions, are possibly caused by a semi-continuous and/or continuous weakly magnetic $Fe_3C$ grain boundary phase. However, some results are contradictory and it is entirely possible that the cause for reduced signal efficiencies has yet to be identified.

- By changing the inspection procedure to use a normal magnetic field of 12 to 14K Gauss, rather than a tangential field wherein magneto-strictive enhancement of ultrasonic signals is necessary, inspection of M549 (RAP) artillery projectiles can be accomplished without requiring changes to current production line procedures. It is thus recommended that the EMAT prototype inspection be designed and constructed accordingly.

- Based on the recommended design change, additional changes will be necessary for constructing this first prototype inspection system. These changes are considered minor and will neither have a significant financial impact on program performance nor influence the capability of the final product to perform reliably. Also, it is not anticipated that this change in inspection procedure will result in a significant financial increase for future systems.

## REFERENCES


1. R. B. Thompson, "Rapid Ultrasonic Inspection of Artillery Projectiles," Rockwell International Science Center Final Report No. SC5067.7FR, Contract No. DAAA25-76-C-0381, January 1977.

2. C. M. Fortunko, R. B. Thompson, and M. W. Mahoney, "Rapid Ultrasonic Inspection of Artillery Projectiles," Rockwell International Science Center Final Report No. SC5113.4FR, Contract No. DAAK10-77-2020, May 1978.

3. R. B. Thompson, "Noncontact Transducers," Ultrasonics Symposium Proceedings, IEEE, p 74, 1977.

4. R. B. Thompson, "Mechanisms of Electromagnetic Generation and Detection of Ultrasonic Lamb Waves in Iron-Nickel Alloy Polycrystals," J. App. Phys., p 4942, December 1977.

5. R. B. Thompson, "Strain Dependence of Electromagnetic Generation of Ultrasonic Surface Waves in Ferrous Metals," App. Phys. Lett., Vol. 28, No. 9, p 483, May 1, 1976.

Table 1. Residual stress results on M549 (RAP) artillery projectiles

| Sample | Depth of Etch (inches) | Stress (ksi) Hoop | Radial | EMAT Ultrasonic Wave Efficiency |
|---|---|---|---|---|
| (A) | | | | |
| OD Surface,(1) | 0 | 27 | 65 | |
| Bourrelet, | .0001 | 35 | 30 | |
| Ground Finish | .0001 | 18 | - | Good |
| | .0001 | 27 | - | |
| | .0016 | -3 | - | |
| | .0030 | 0 | - | |
| (B) | | | | |
| OD Surface,(1) | 0 | -47 | -48 | |
| Ogive | .0001 | -62 | -55 | |
| Hot Worked Surface | .0010 | -62 | -64 | |
| | .0027 | -62 | -62 | |
| | .0040 | -62 | - | Poor |
| | .0066 | -62 | - | |
| | .0092 | -54 | -48 | |
| | .0103 | -45 | -36 | |
| | .0113 | -32 | -33 | |
| (C) | | | | |
| ID Surface,(1) | .0001 | -40 | | |
| Ogive, | .0016 | -38 | | Good |
| Hot Worked Surface | .0032 | -28 | | |
| | .0059 | -13 | | |
| (D) | | | | |
| OD Surface,(1) | 0 | -55 | | |
| Ogive | .0001 | -65 | | Good |
| Carburized | .0010 | -82 | | |
| | .0025 | -75 | | |
| (E) | | | | |
| OD Surface,(1) | 0 | -56 | | |
| Ogive | .0001 | -51 | | Poor |
| Decarburized | .0015 | -75 | | |

Table 1 (Continued)

| Sample | Depth of Etch (inches) | Stress (ksi) Hoop | Radial | EMAT Ultrasonic Wave Efficiency |
|---|---|---|---|---|
| (F) | | | | |
| OD Surface,(1) | 0 | -47 | | |
| Bourrelet | .001 | -64 | | Good |
| Carburized | .003 | -37 | | |
| (G) | | | | |
| OD Surface,(2) | 0 | -52 | | |
| Ogive | .001 | -71 | | |
| Hot Worked Surface | .002 | -65 | | |
| | .004 | -66 | | Poor |
| | .006 | -65 | | |
| | .008 | -65 | | |
| | .010 | -55 | | |
| | .013 | -33 | | |
| (H) | | | | |
| OD Surface,(2) | 0 | -21 | | |
| Ogive | 0 | 0 | | |
| Before Heat-Treatment | 0 | -5 | | Good |
| | .003 | -10 | | |
| | .007 | -10 | | |
| (I) | | | | |
| OD Surface,(2) | .003 | -77 | | |
| Ogive | .007 | -77 | | Poor |
| After Heat-Treatment | .011 | -80 | | |

(1) Projectiles manufactured during 1975.
(2) Projectiles manufactured during 1978.

Table 2 Electrodischarge machined notches located on the OD surface of an M549 (RAP) projectile

| Notch[1] Position | Notch[2] Length (in.) | Notch[3] Depth (in.) |
|---|---|---|
| 1 | 0.426 | 0.008 |
| 2 | 0.464 | 0.010 |
| 3 | 0.457 | 0.020 |
| 4 | 0.628 | 0.036 |
| 5 | 0.490 | 0.016 |
| 6 | 0.539 | 0.018 |
| 7 | 0.565 | 0.017 |
| 8 | 0.431 | 0.015 |
| 9 | 0.357 | 0.009 |
| 10 | 0.463 | 0.019 |

(1) See Fig. 20a for notch location on an M-549 (RAP) artillery projectile.
(2) Notch length is parallel to the long axis of projectiles.
(3) Notch Radius = 1.25 in.

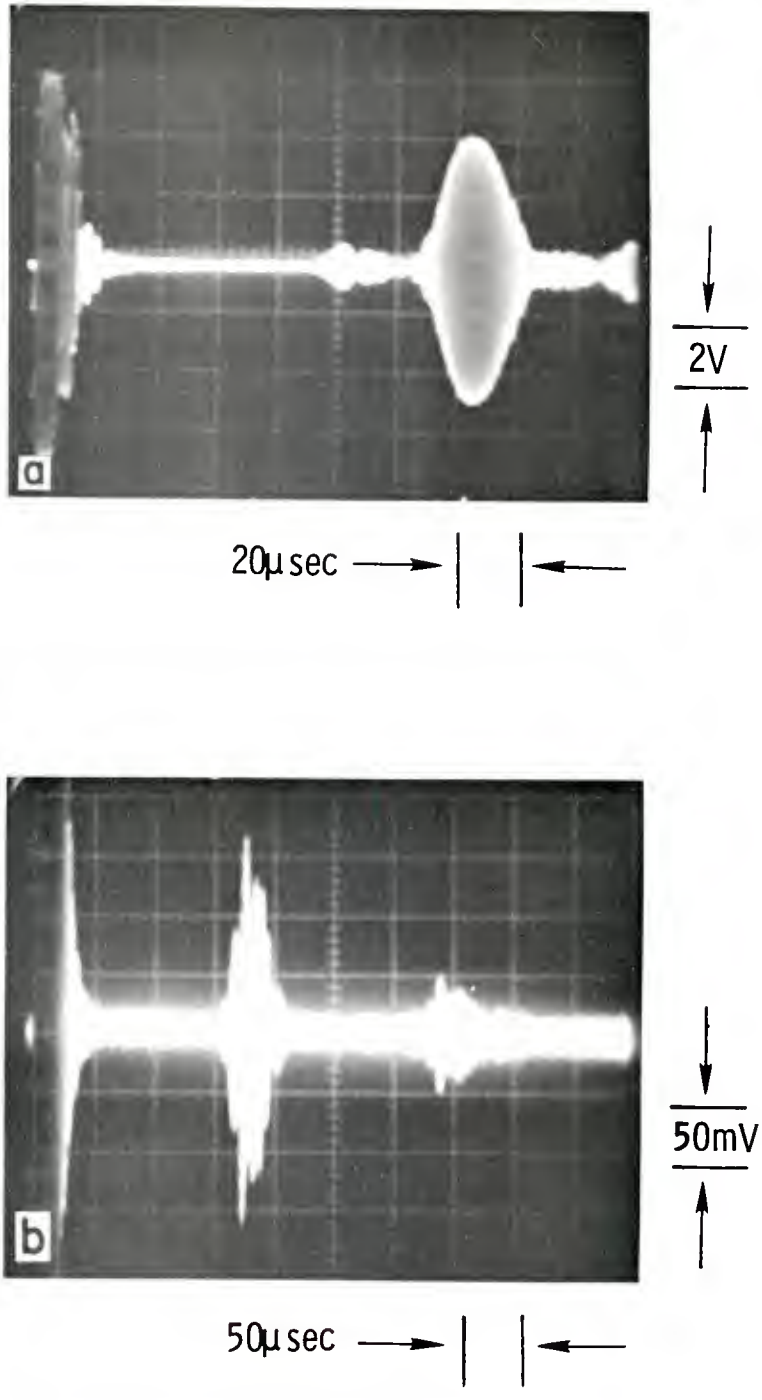


Fig. 1 EMAT ultrasonic signal efficiency for different locations on an M549 (RAP) artillery projectile. (a) Machined bourrelet and (b) hot worked ogive.

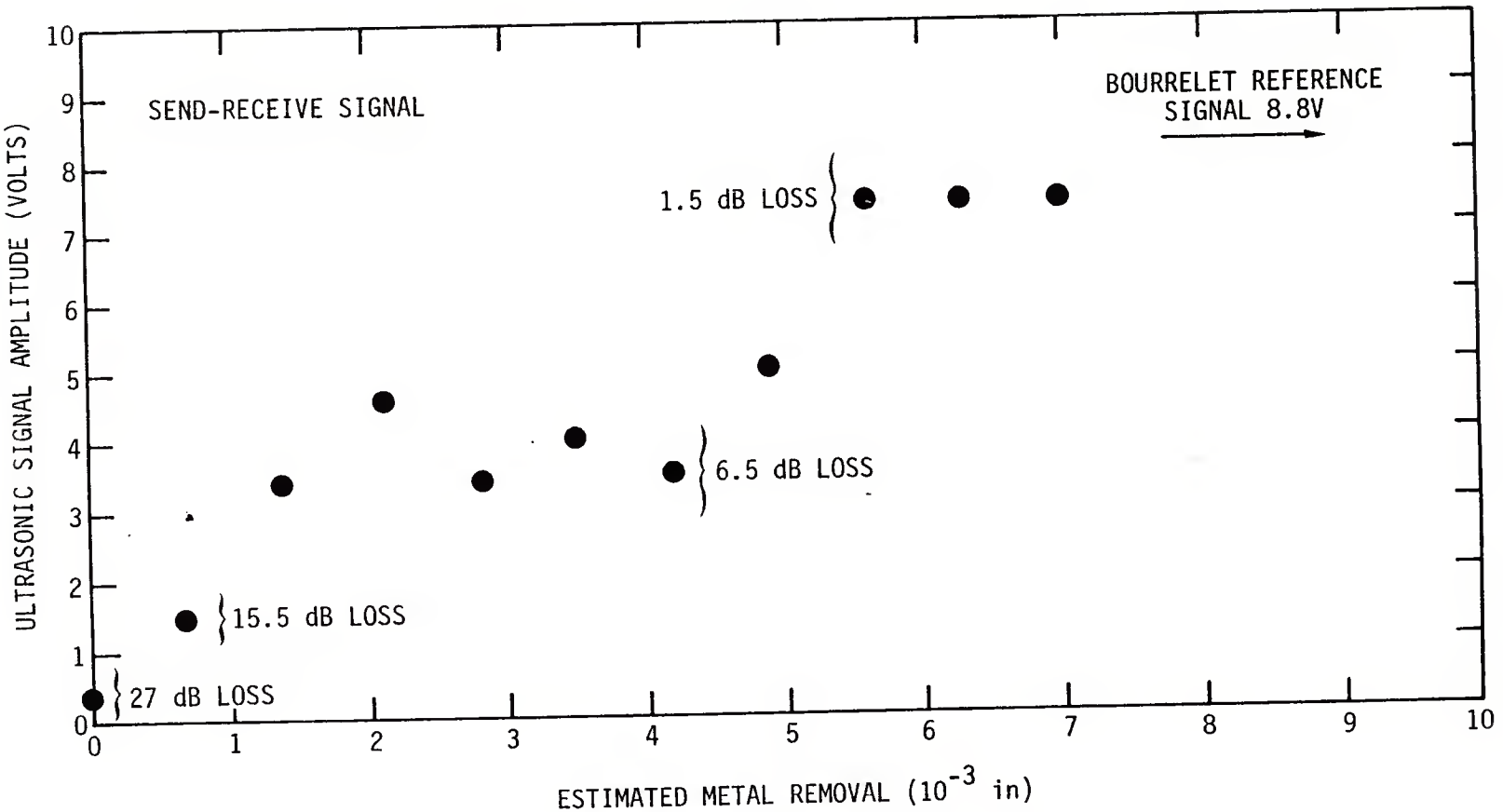


Fig. 2 EMAT transducer efficiency as a function of metal removed from the ogive of an M-549 artillery projectile.

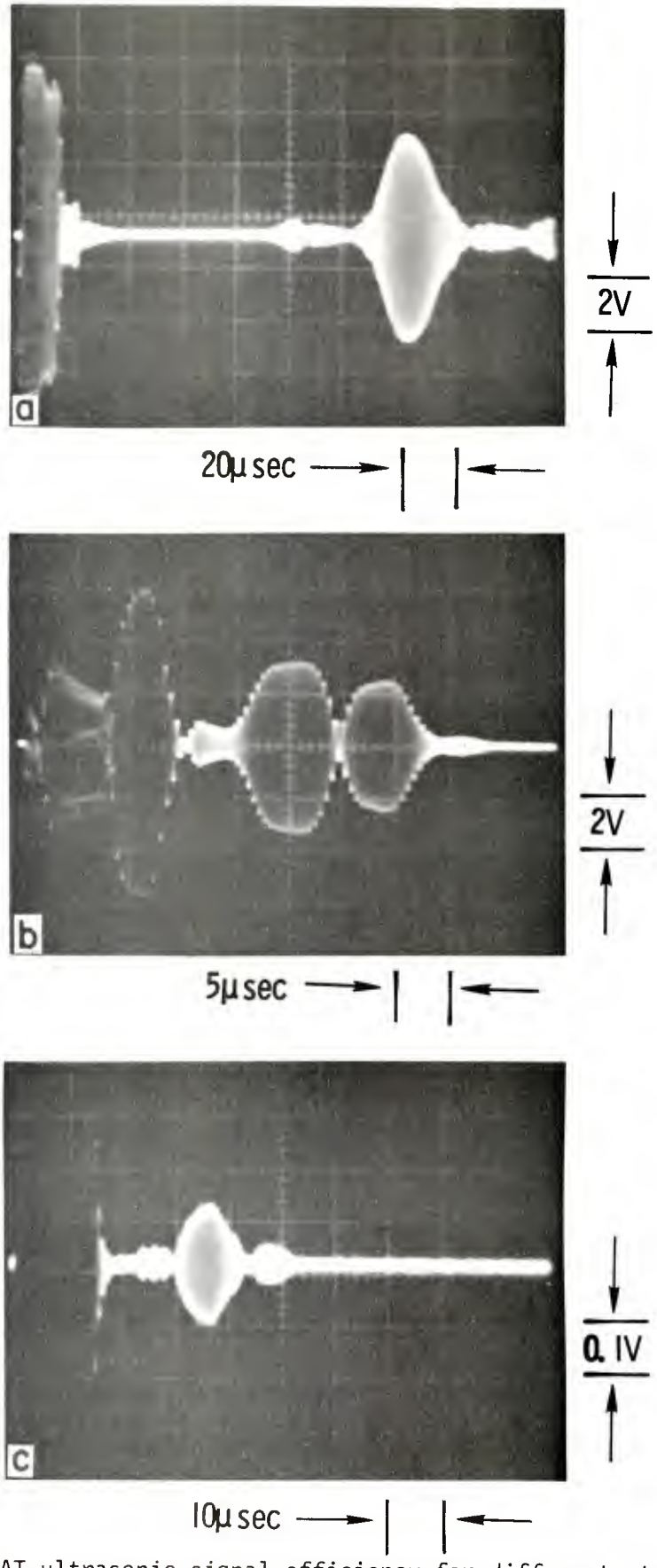


Fig. 3 EMAT ultrasonic signal efficiency for different stages of fabrication of an M549 (RAP) artillery projectile. (a) Prior to nosing, (b) prior to heat treatment and (c) after heat treatment.

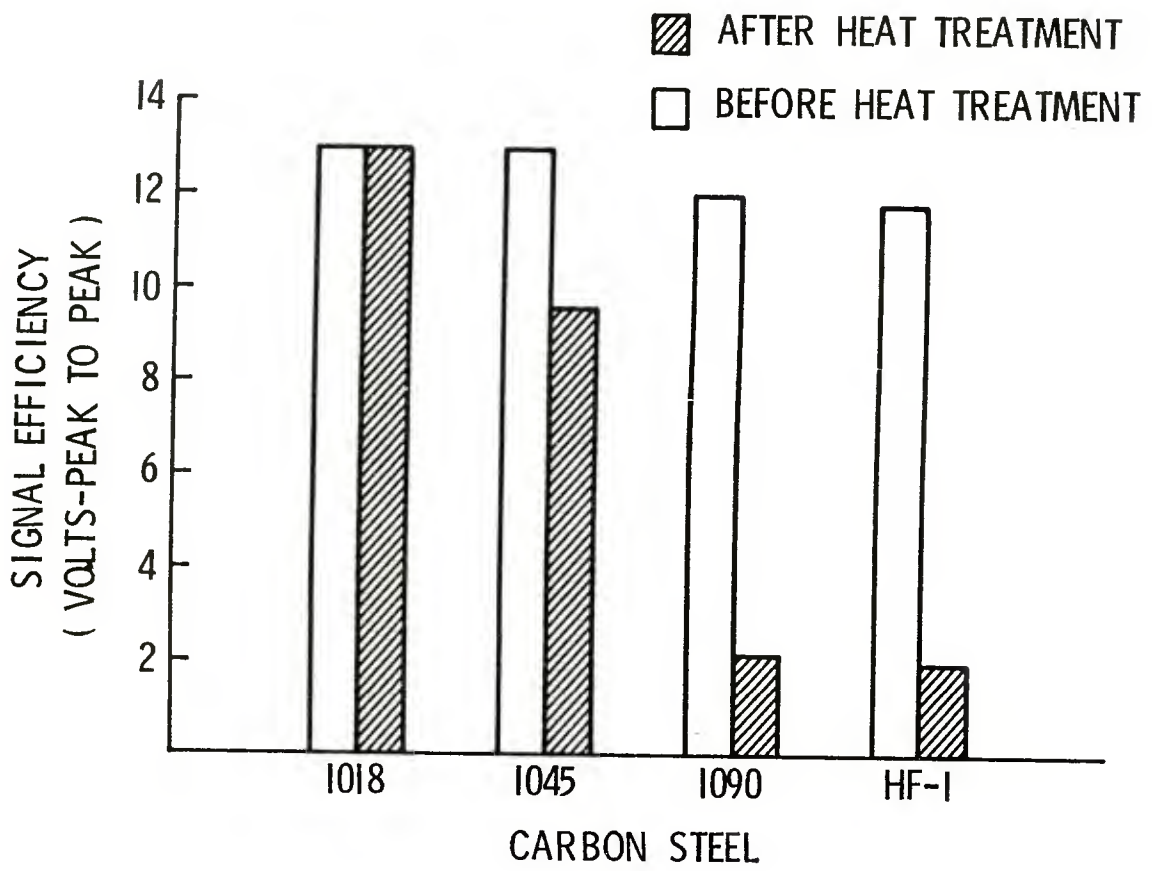


Fig. 4 EMAT ultrasonic signal efficiency as a function of carbon content and carbide morphology.

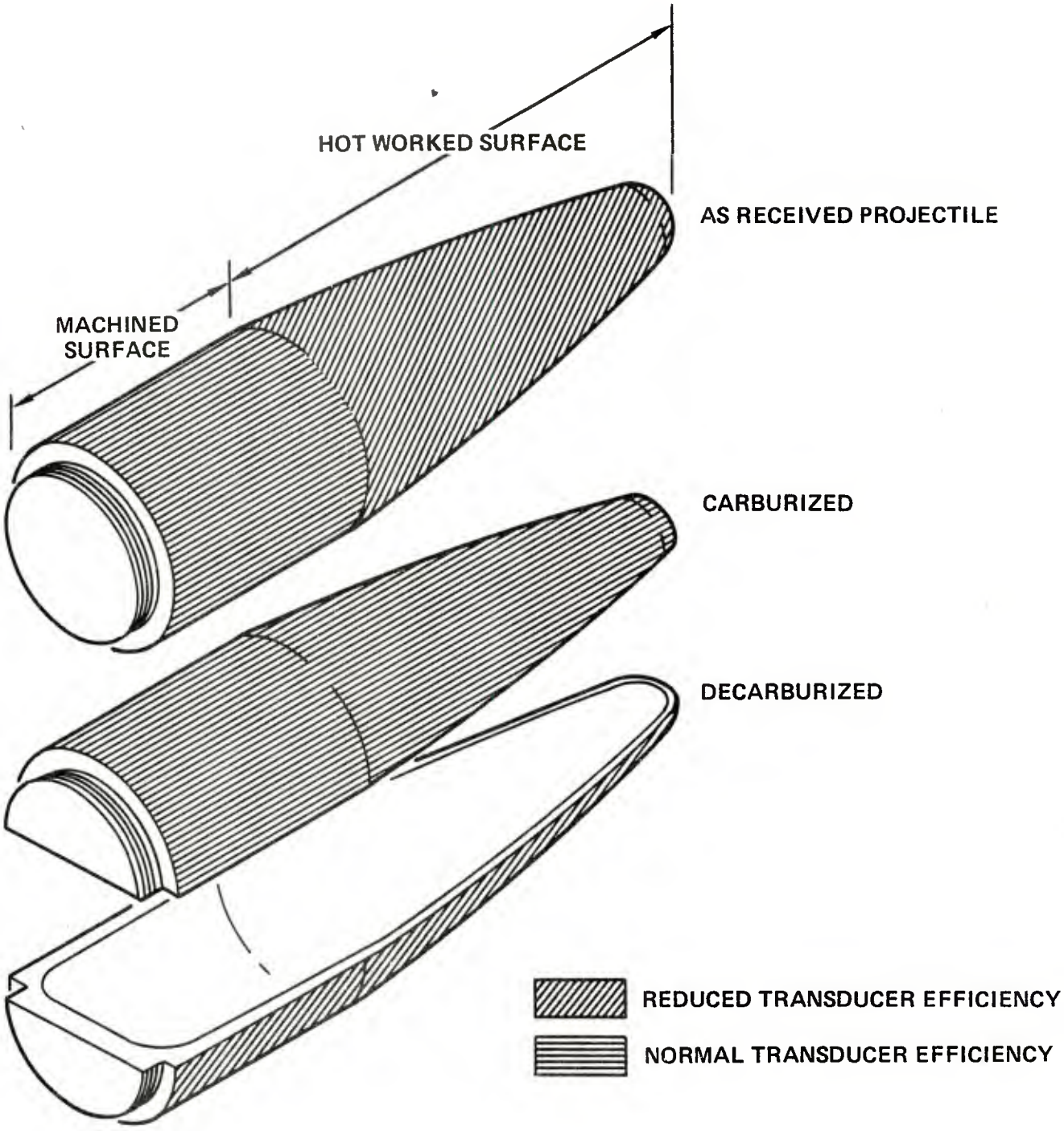


Fig. 5 Changes in transducer efficiency as a function of surface condition and heat treatment.

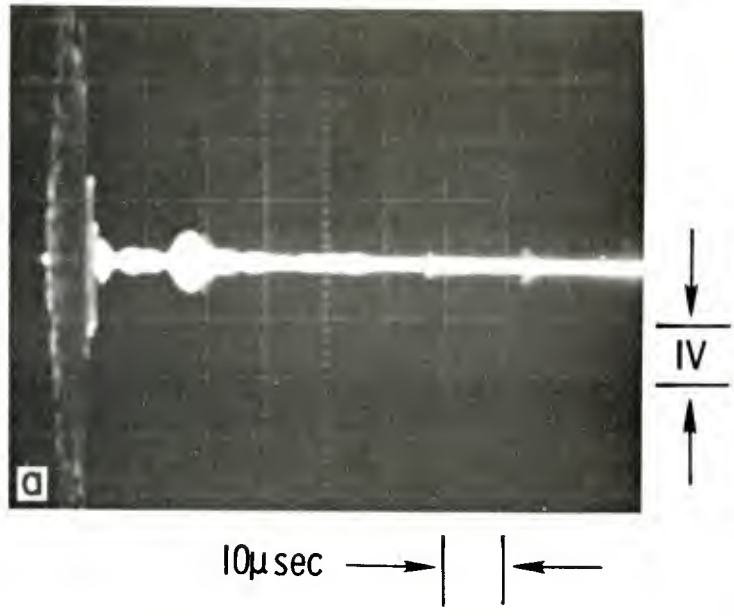


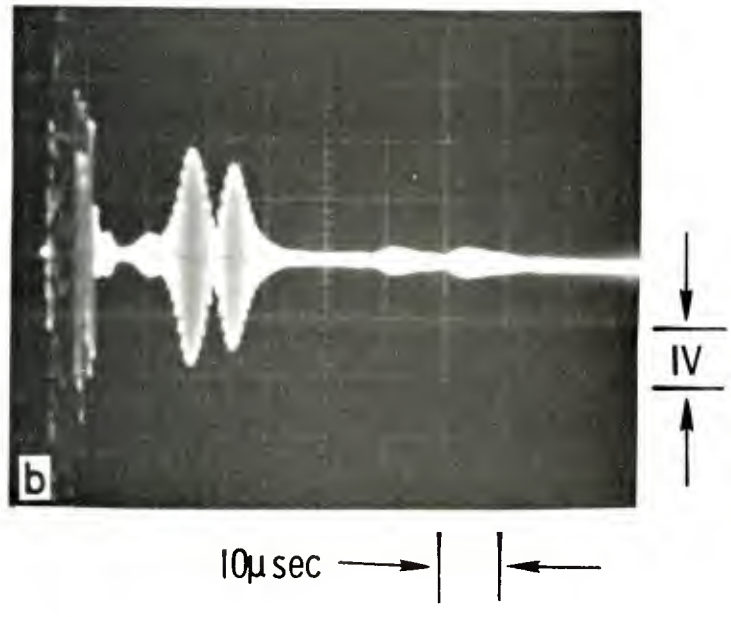


Fig. 6 EMAT ultrasonic signal efficiency on an M549 (RAP) artillery projectile after (a) decarburization and (b) carburization.

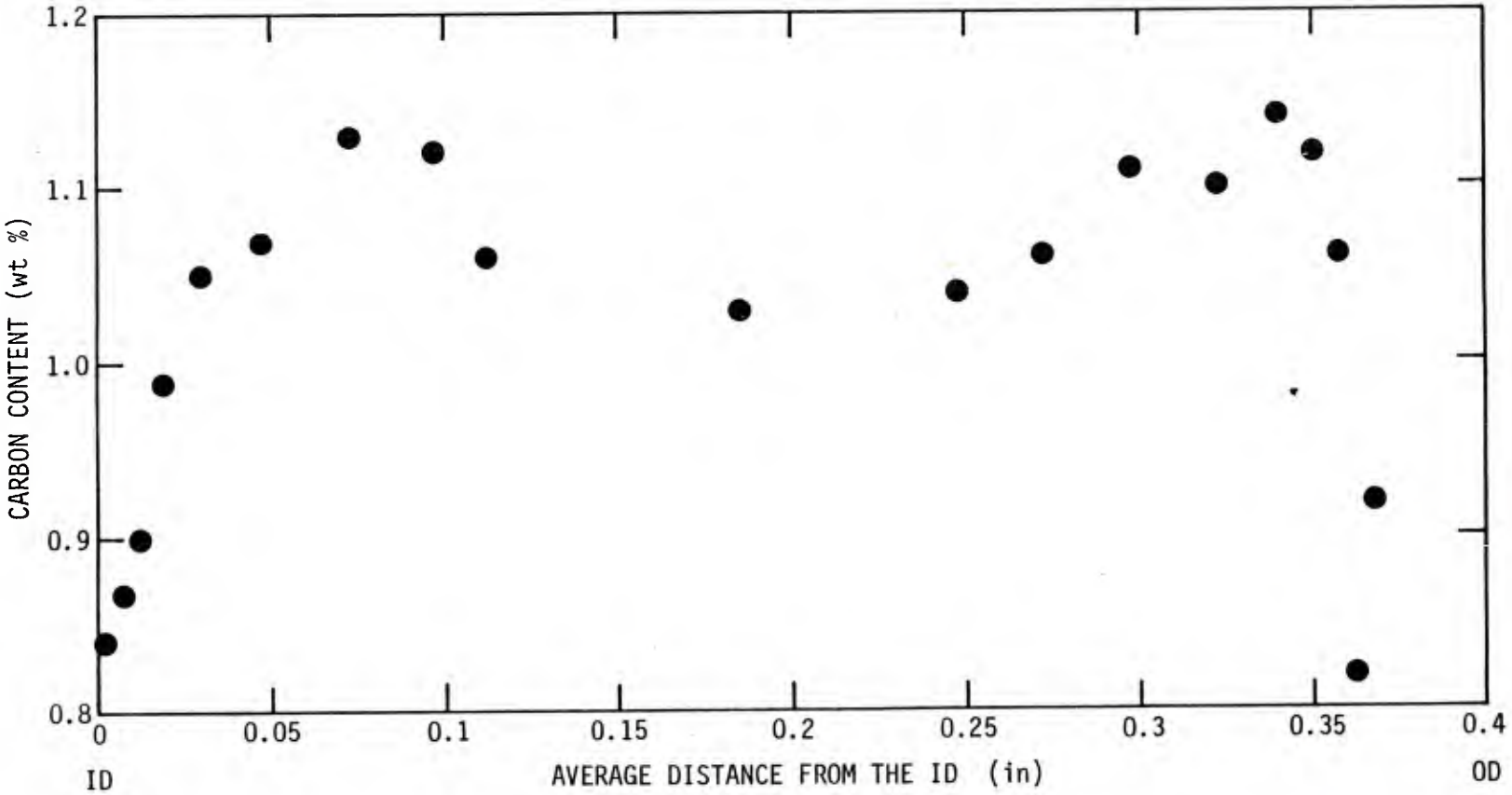


Fig. 7 Carbon analysis through the wall thickness in the ogive of an M-549 artillery projectile.

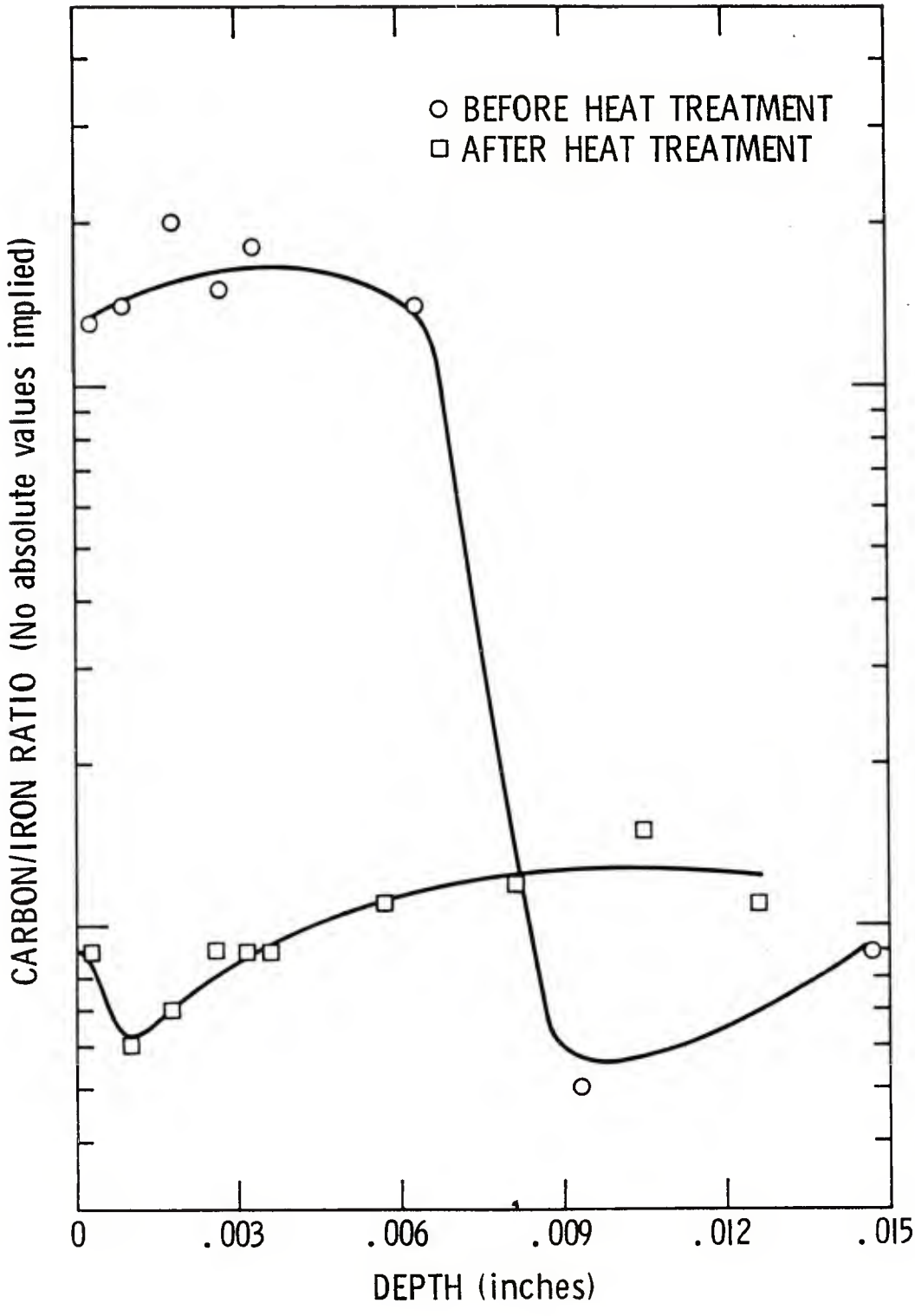


Fig. 8 Chemical analysis by Auger spectroscopy illustrating the C/Fe ratio as a function of depth below the surface and heat treatment.

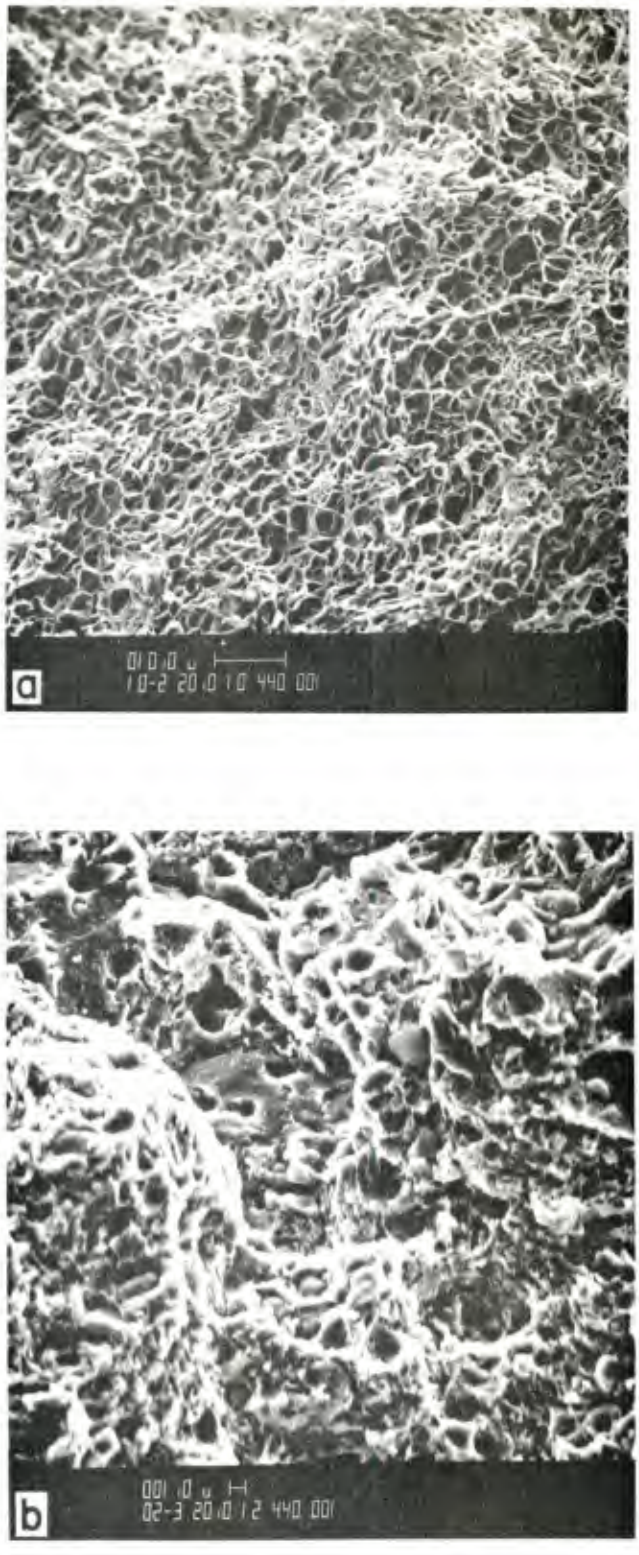


Fig. 9 Scanning electron microscopy illustrating fracture modes of an M549 (RAP) artillery projectile (a) before heat treatment and (b) after heat treatment.

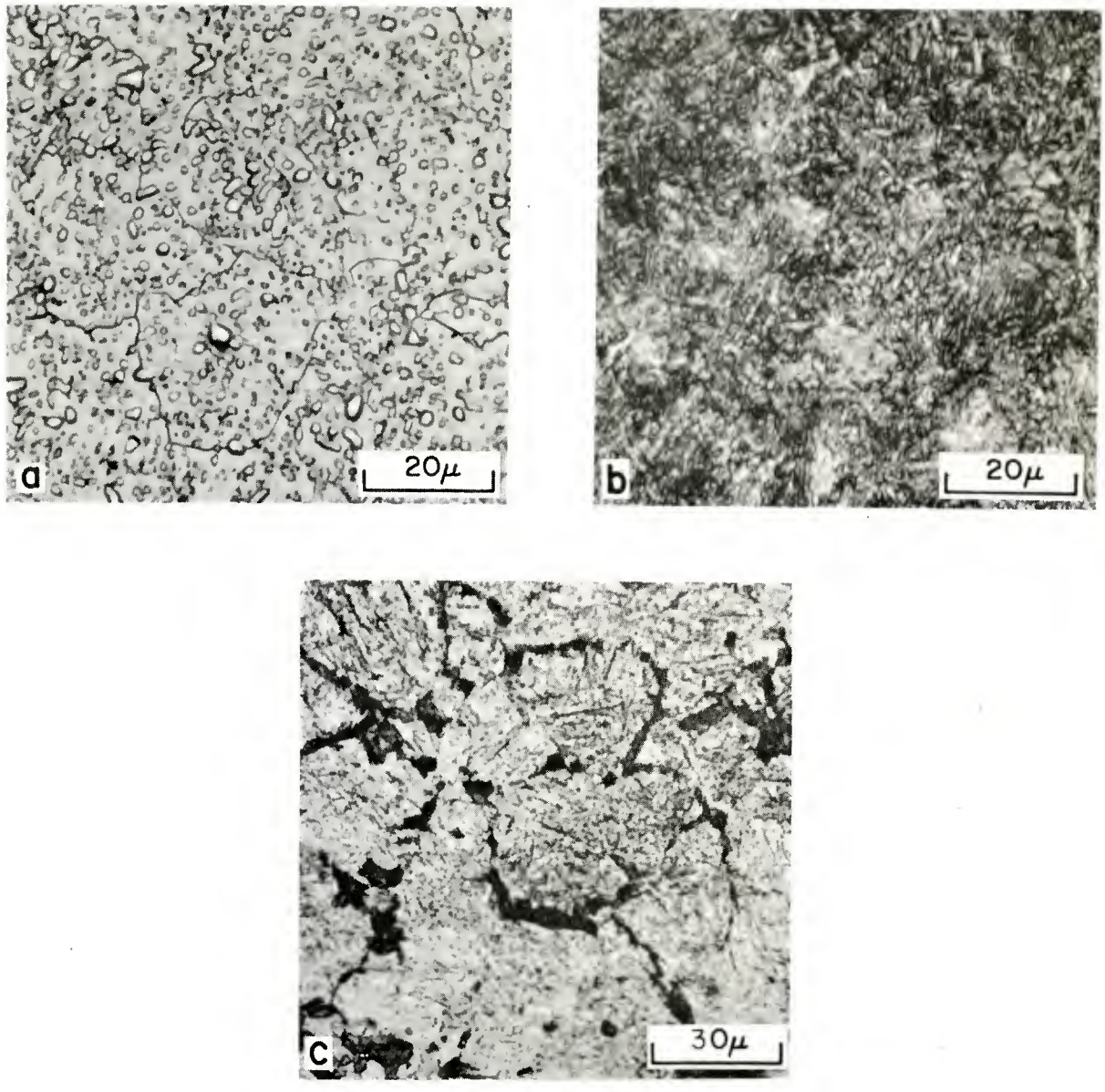


Fig. 10 Metallography of 1090 steel illustrating microstructures (a) before heat treatment, (b) after heat treatment and (c) after heat treatment and near the surface of the specimen.

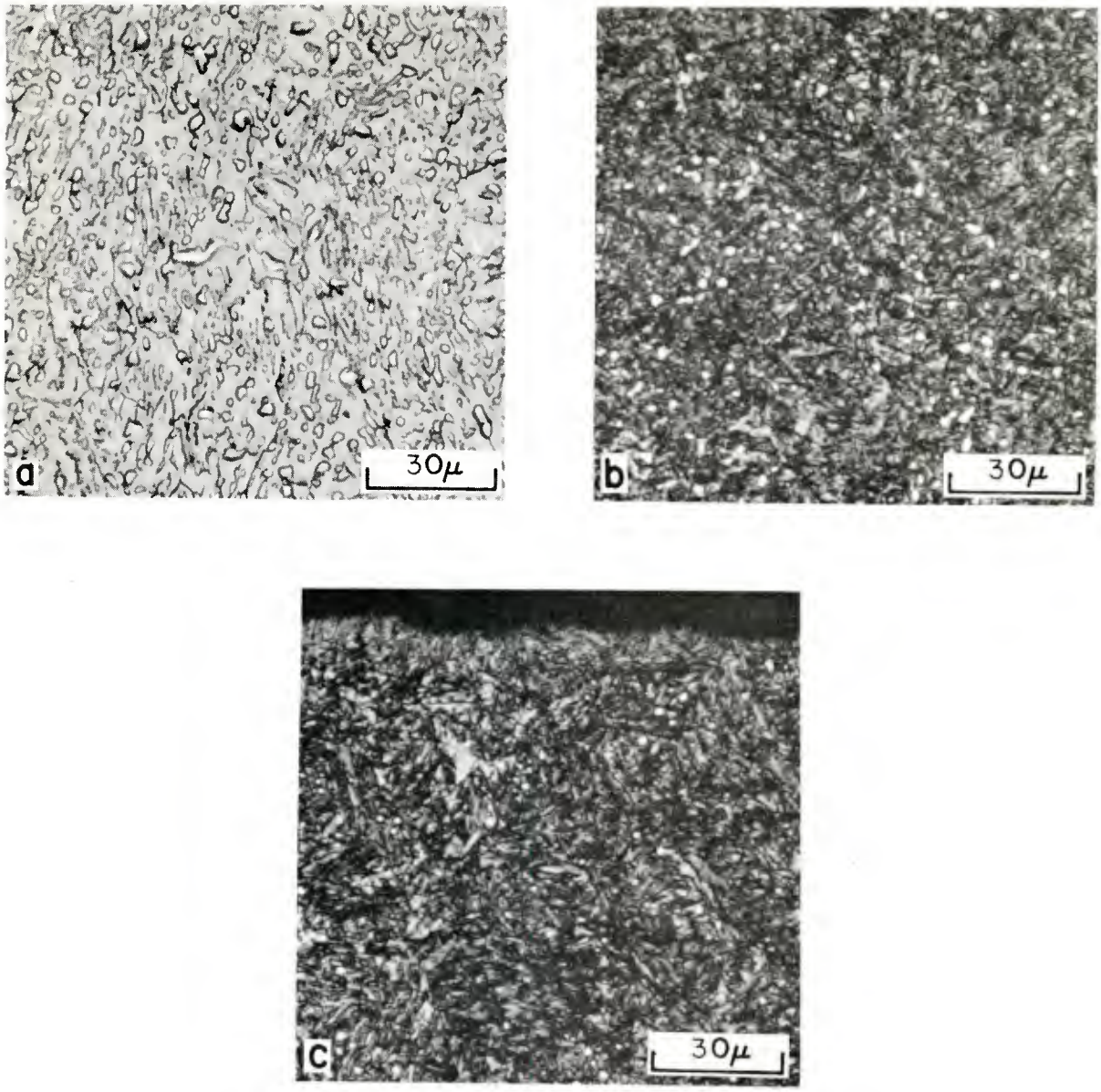


Fig. 11 Metallography of an M549 (RAP) artillery projectile illustrating microstructures (a) before heat treatment, (b) after heat treatment and (c) after heat treatment and near the surface of the specimen.

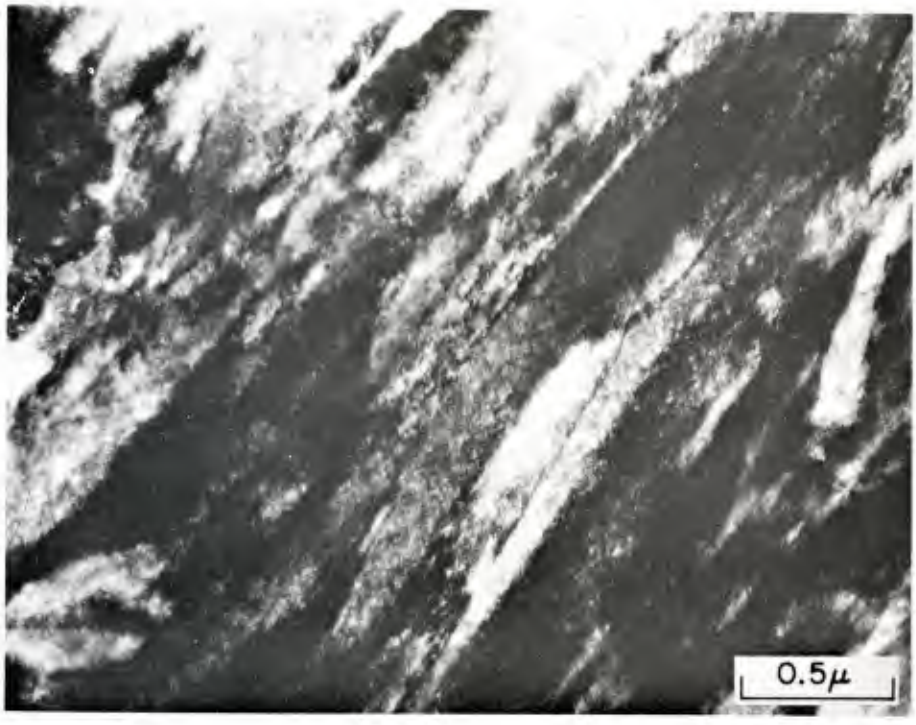


Fig. 12 Transmission electron microscopy of 1045 steel after heat treatment illustrating the absence of precipitated carbides.

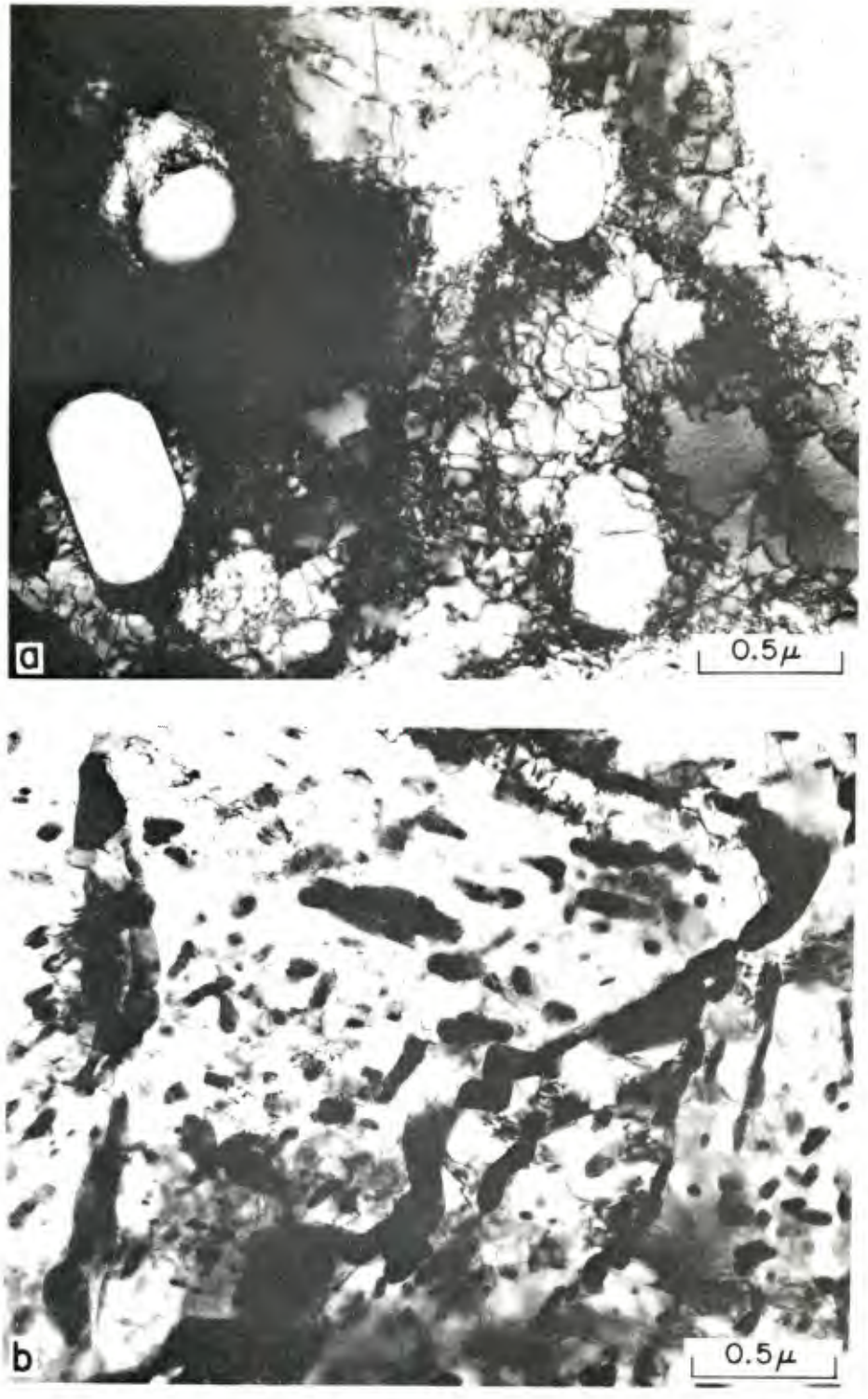


Fig. 13 Transmission electron microscopy of 1090 steel illustrating (a) discrete carbide precipitates prior to heat treatment and (b) semicontinuous and continuous grain boundary carbides as a result of heat treatment.

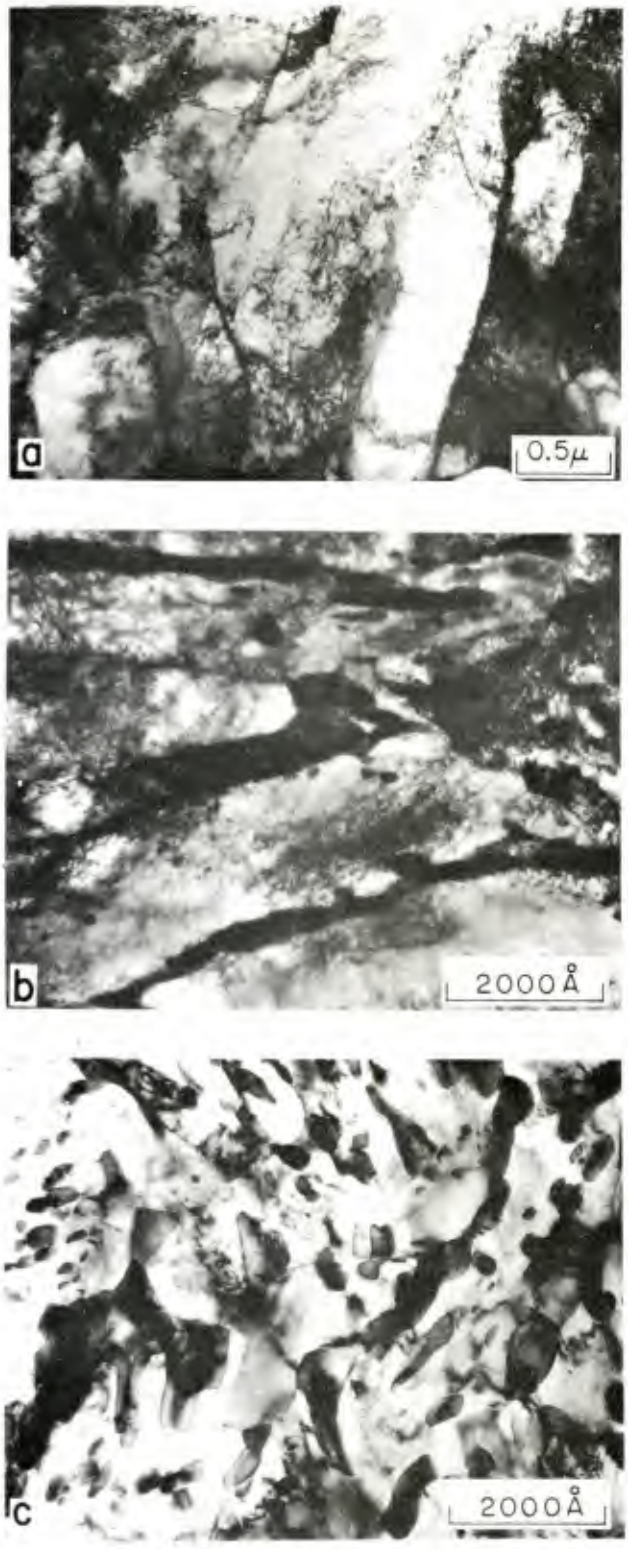


Fig. 14 Transmission electron microscopy of HF-1 steel illustrating (a) the absence of carbide precipitates prior to heat treatment, (b) continuous grain boundary carbide precipitates near the surface following heat treatment and (c) semi-continuous and continuous grain boundary carbide precipitates some distance from the surface.

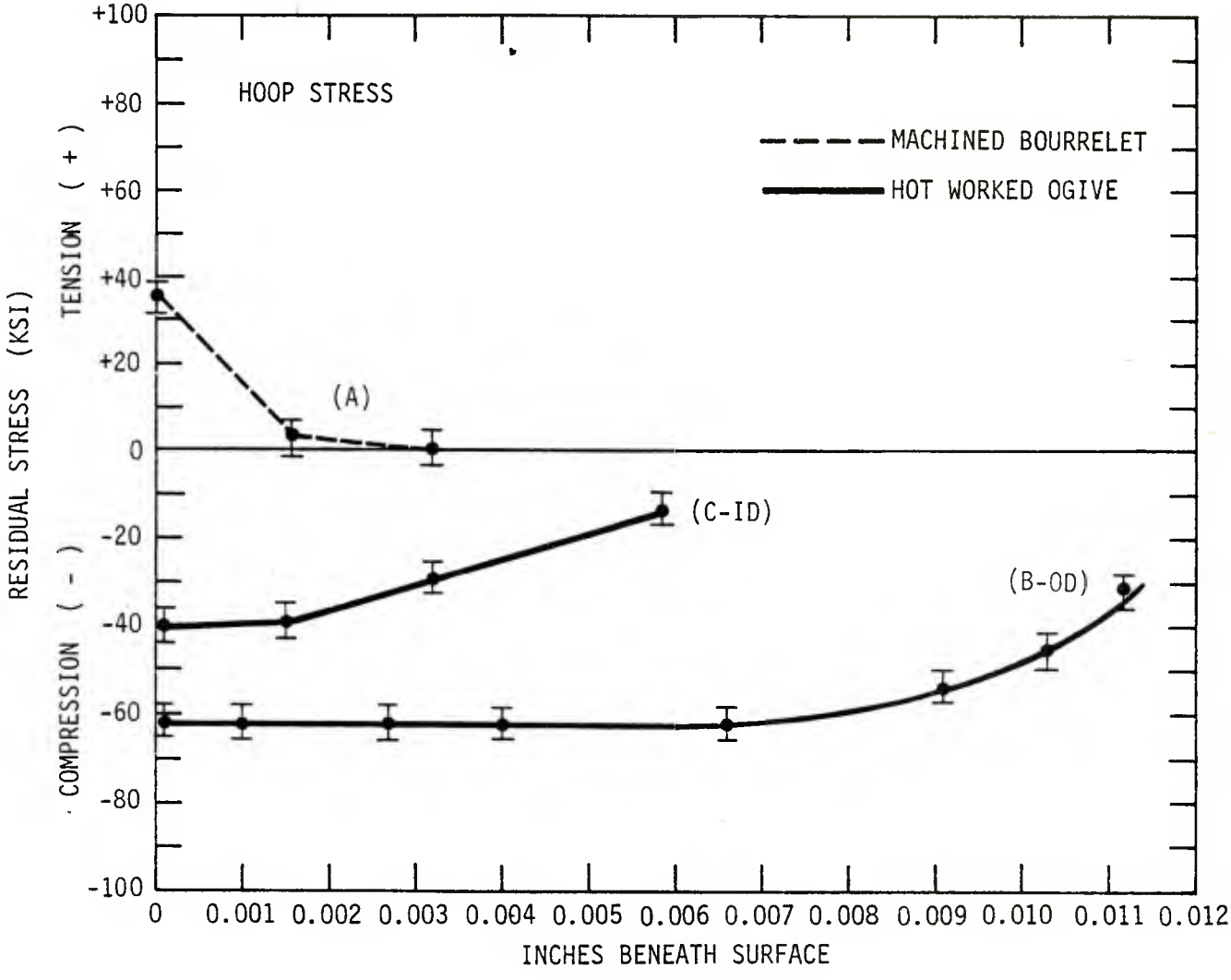


Fig. 15 Residual stress measurements by x-ray diffraction as a function of metal removed from the OD surface on an M549 artillery projectile.

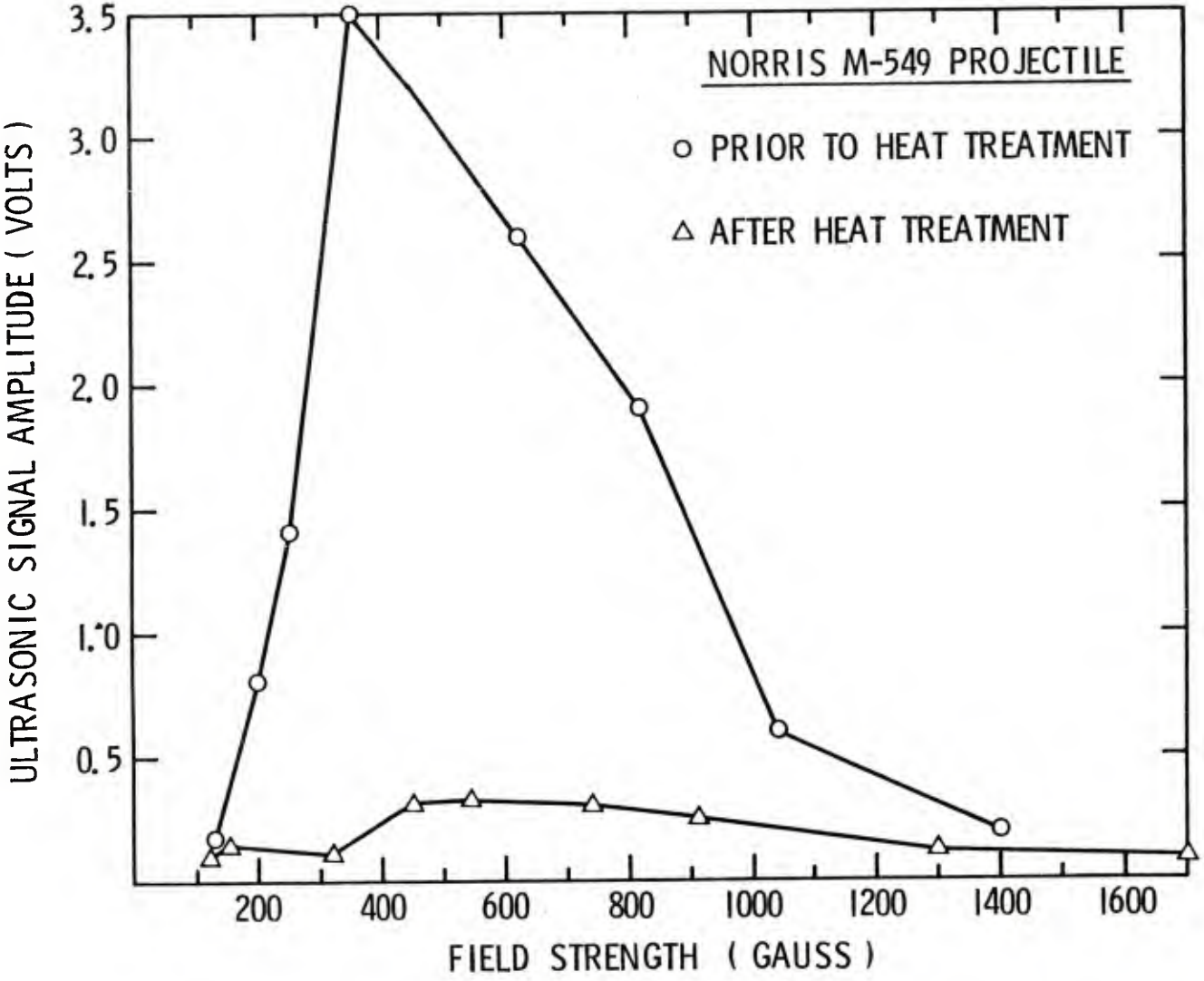


Fig. 16 EMAT ultrasonic signal amplitude on an M549 (RAP) artillery projectile in a tangential magnetic field before and after heat treatment.

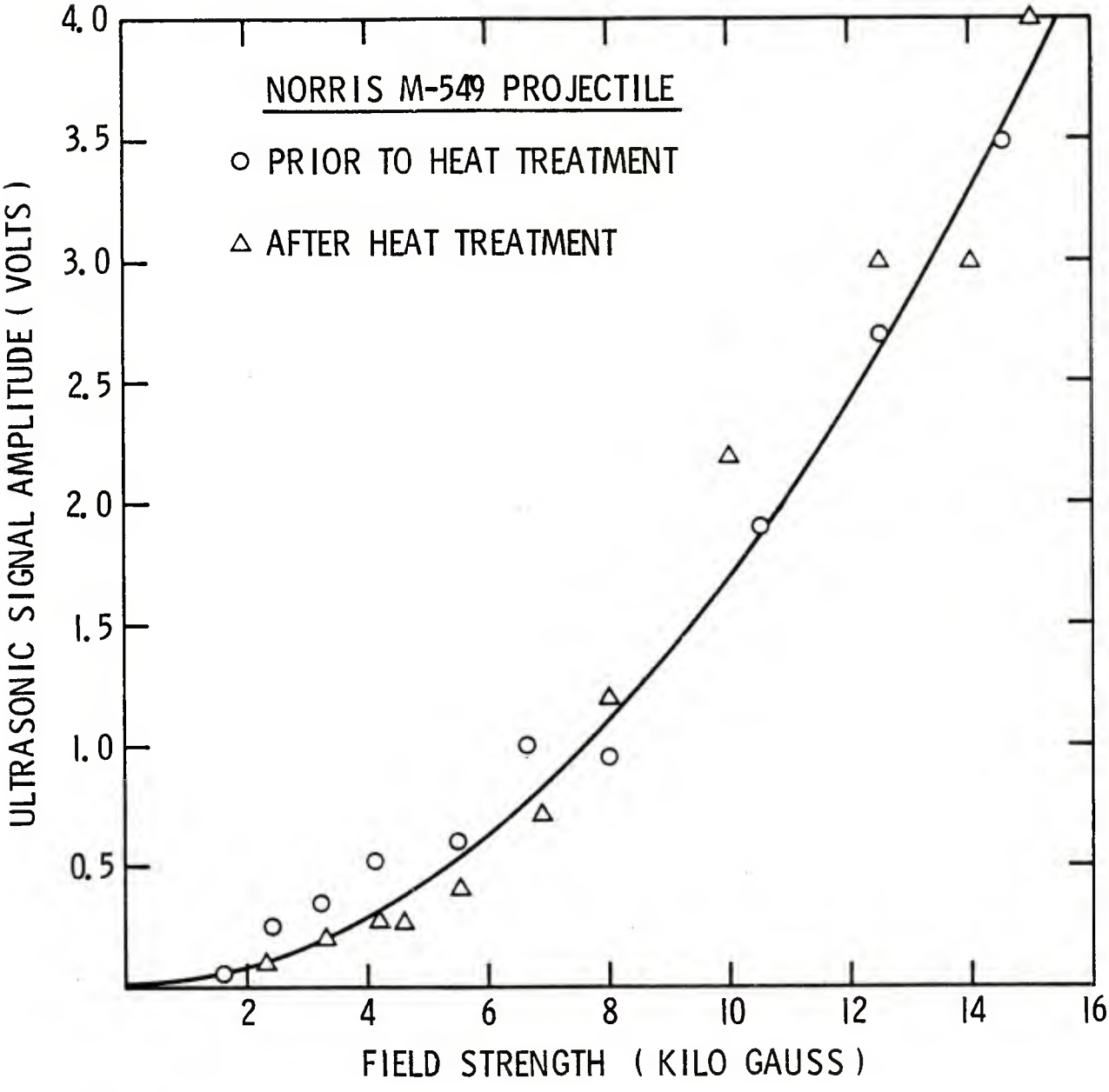


Fig. 17 EMAT ultrasonic signal amplitude of an M549 (RAP) artillery projectile in a normal magnetic field before and after heat treatment.

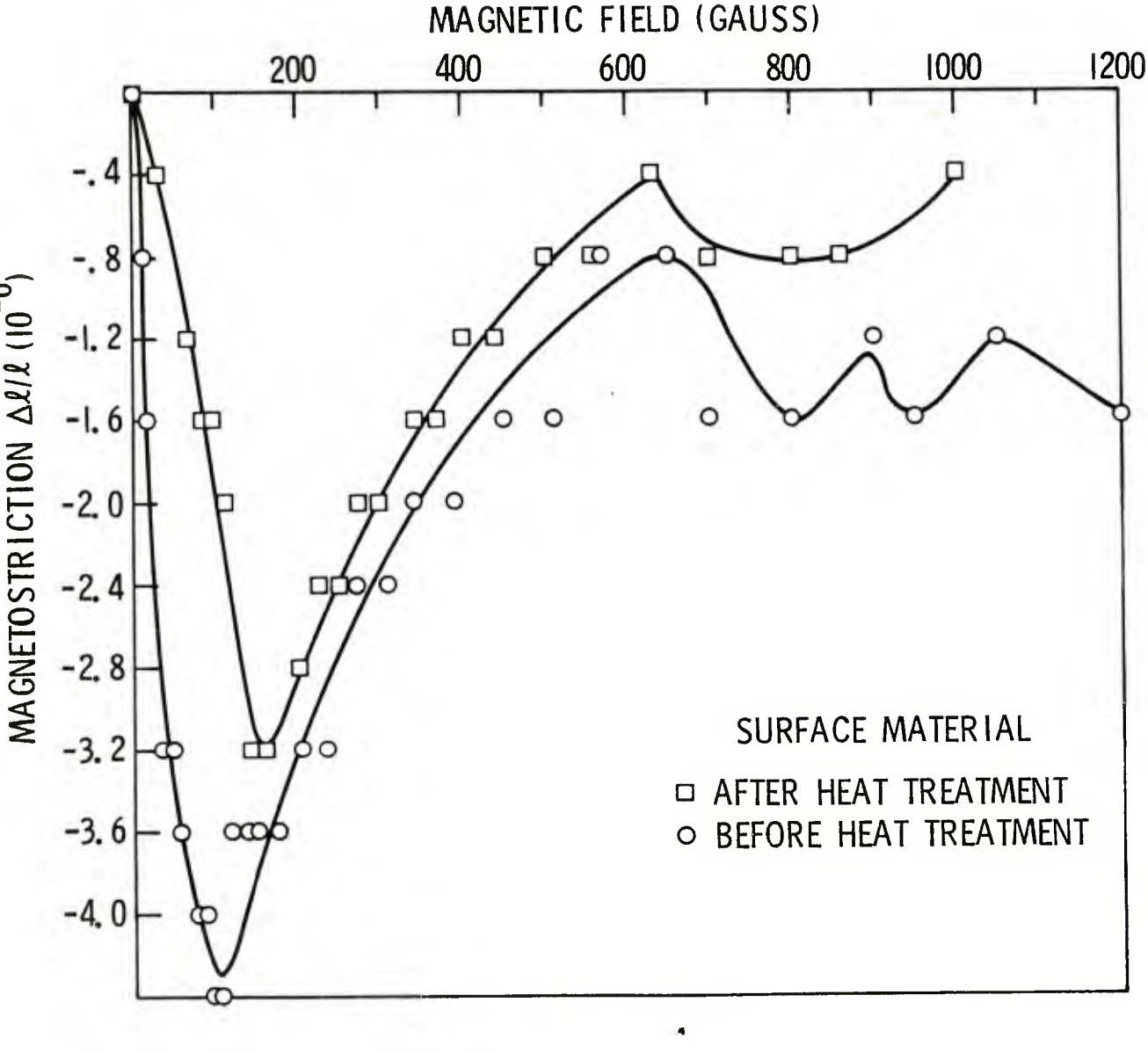


Fig. 18 Magnetostrictive strain as a function of applied magnetic field for material 0.007 inch from the OD surface of an M549 (RAP) projectile.

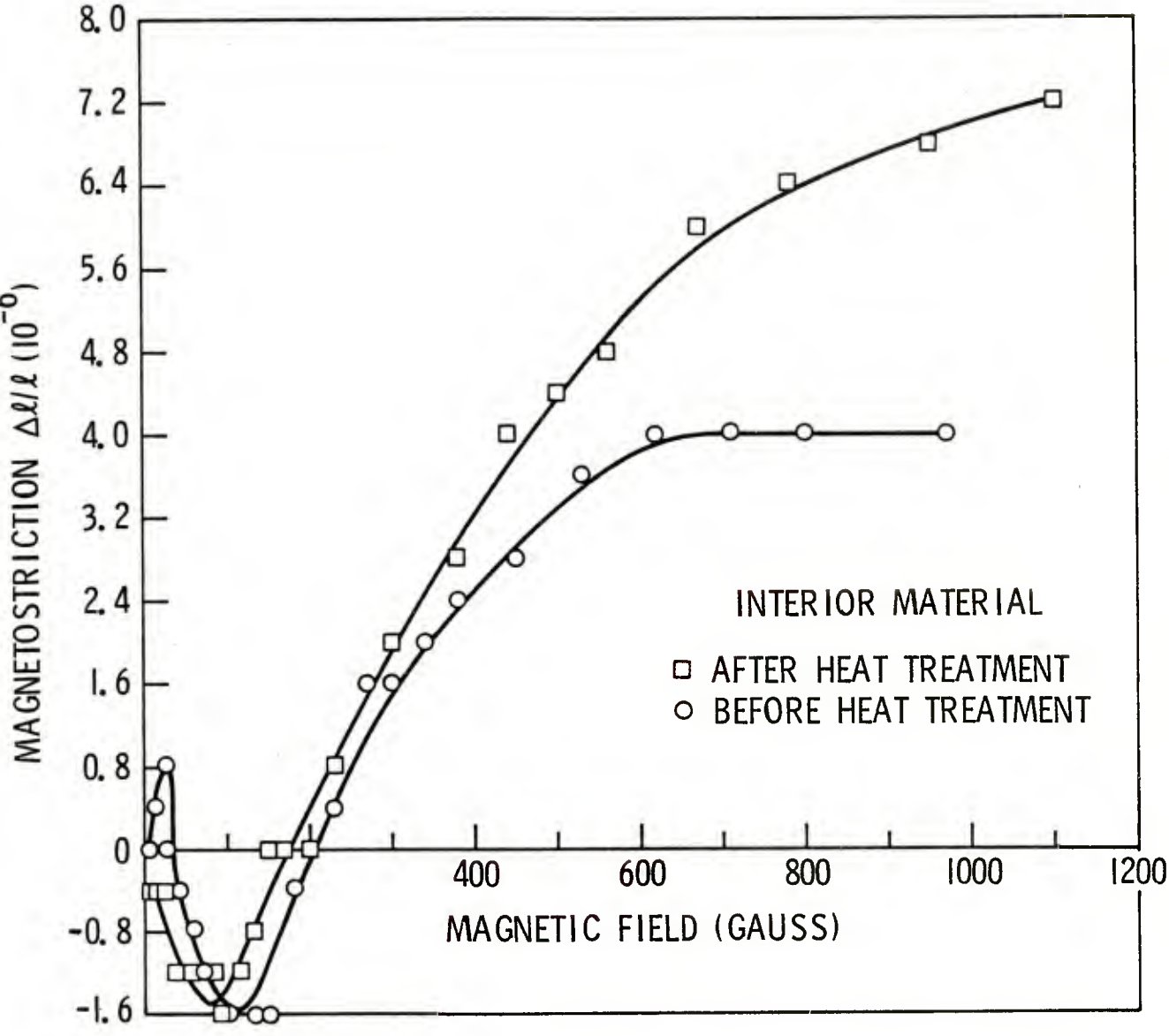


Fig. 19 Magnetostrictive strain as a function of applied magnetic field for HF-1 steel.

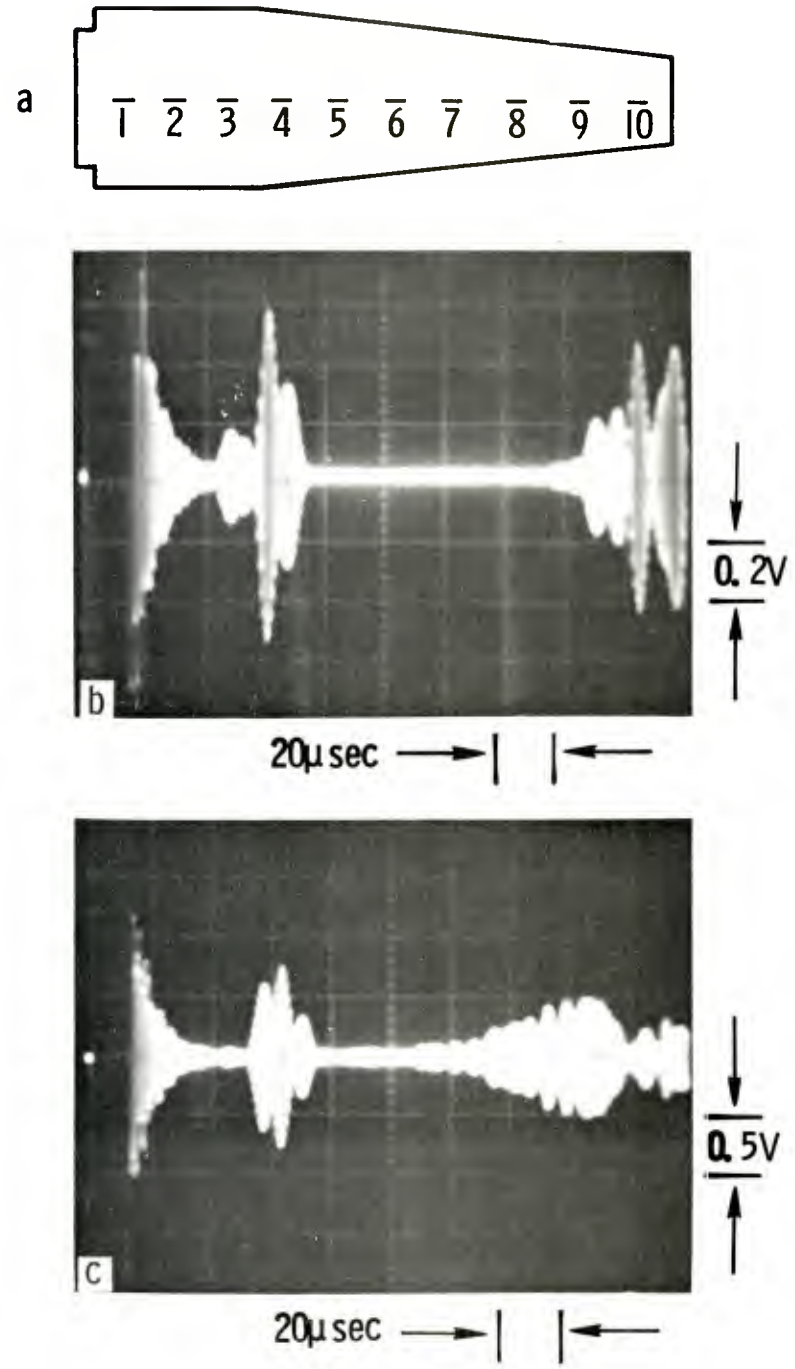


Fig. 20 Illustration of EMAT ultrasonic signal amplitude for EDM notch sizes tabulated in table 2. (a) location of OD longitudinal notches on an M549 (RAP) artillery projectile, (b) location 2, (c) location 3.

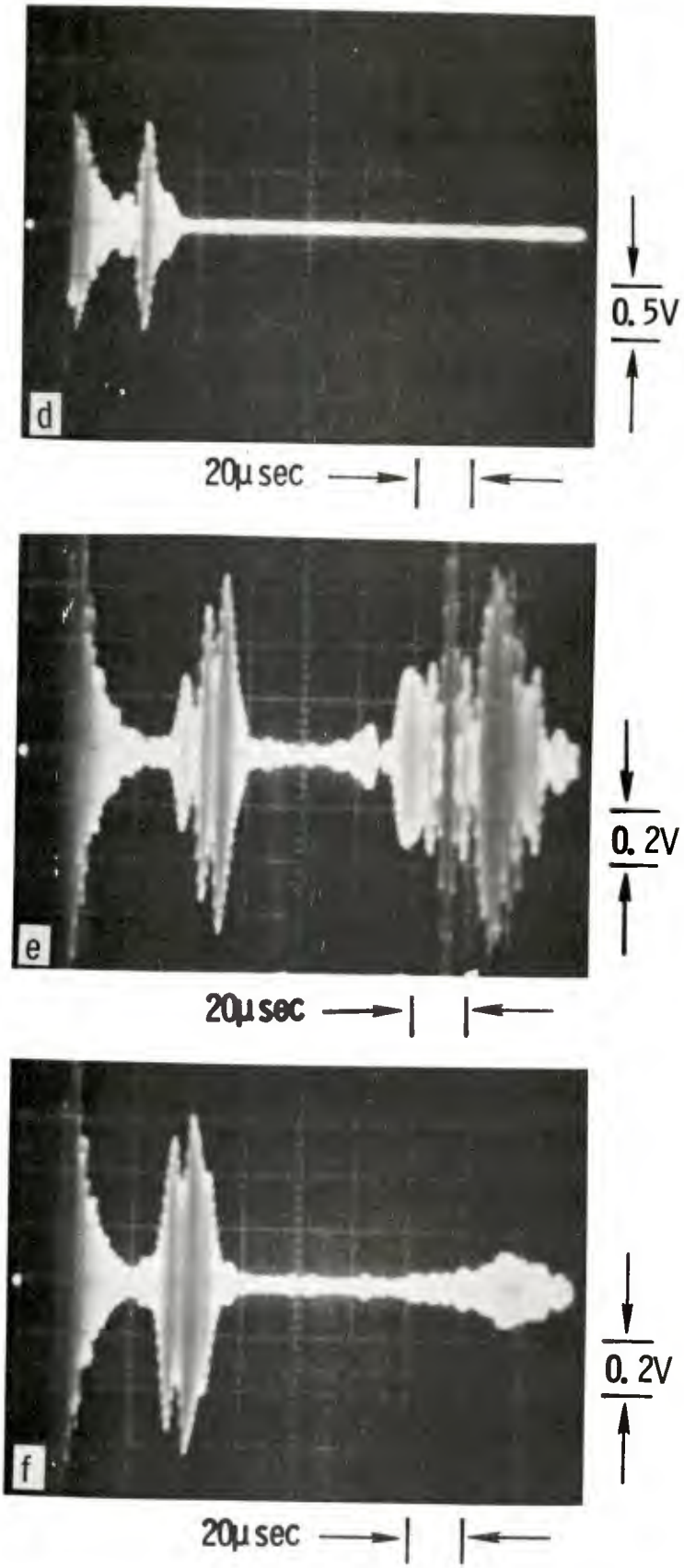


Fig. 20 Continued - (d) location 4, (e) location 5, (f) location 6.

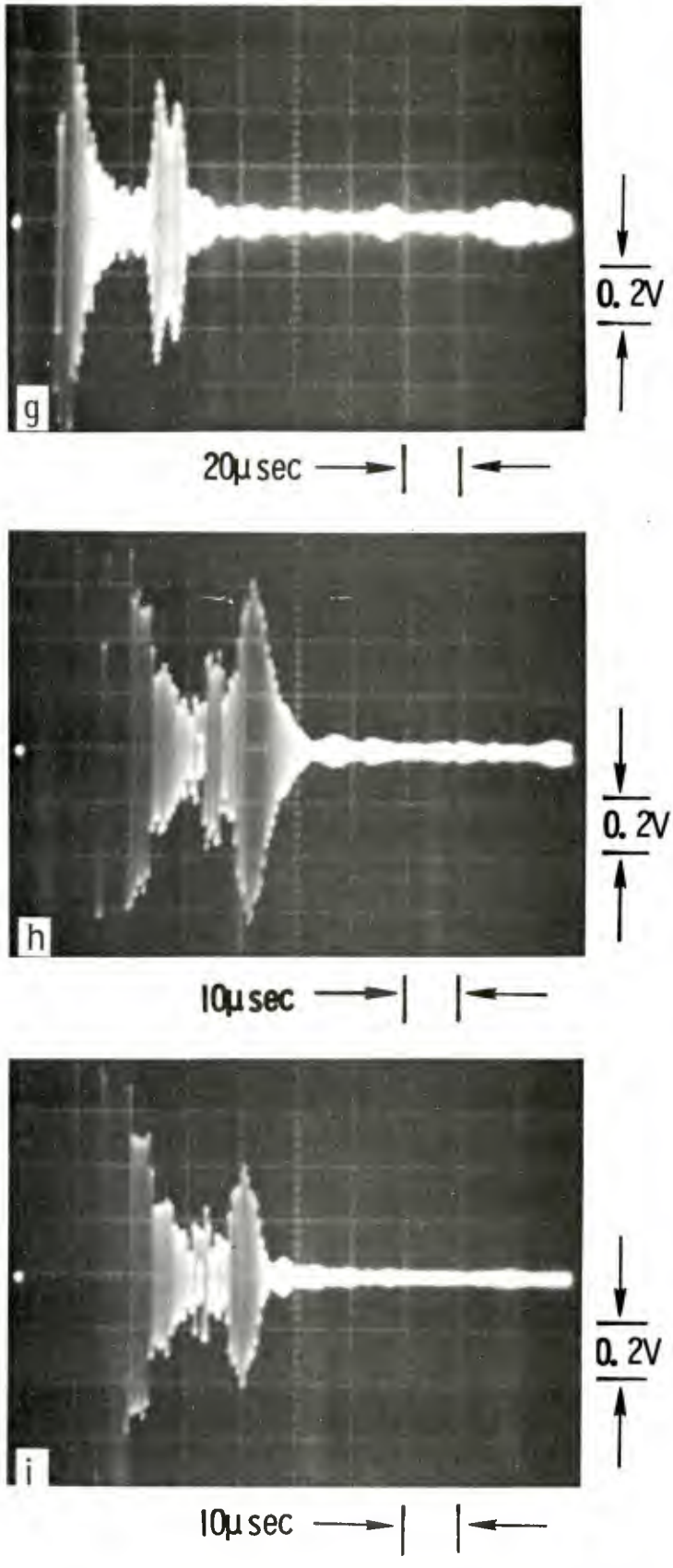


Fig. 20 Continued - (g) location 7, (h) location 8, (i) location 9.

# TABLE OF EQUIVALENTS

## Length

| Inch | Metre |
|---|---|
| 0.0001 | 2.540 E-06 |
| 0.0010 | 2.540 E-05 |
| 0.0015 | 3.810 E-05 |
| 0.0016 | 4.064 E-05 |
| 0.0020 | 5.080 E-05 |
| 0.0025 | 6.350 E-05 |
| 0.0027 | 6.858 E-05 |
| 0.0030 | 7.620 E-05 |
| 0.0032 | 8.128 E-05 |
| 0.0040 | 1.016 E-04 |
| 0.0050 | 1.270 E-04 |
| 0.0060 | 1.524 E-04 |
| 0.0066 | 1.676 E-04 |
| 0.0070 | 1.778 E-04 |
| 0.0080 | 2.032 E-04 |
| 0.0097 | 2.464 E-04 |
| 0.0100 | 2.540 E-04 |
| 0.0110 | 2.794 E-04 |
| 0.0113 | 2.870 E-04 |
| 0.0120 | 3.048 E-04 |
| 0.0130 | 3.302 E-04 |
| 0.0150 | 3.810 E-04 |
| 0.0500 | 1.270 E-03 |
| 0.1000 | 2.540 E-03 |
| 0.1500 | 3.81 E-03 |
| 0.2000 | 5.08 E-03 |
| 0.250 | 6.35 E-03 |
| 0.300 | 7.620 E-03 |
| 0.350 | 8.890 E-03 |
| 0.357 | 9.067 E-03 |
| 0.426 | 1.082 E-02 |
| 0.431 | 1.095 E-02 |
| 0.457 | 1.161 E-02 |
| 0.463 | 1.176 E-02 |
| 0.464 | 1.179 E-02 |
| 0.490 | 1.245 E-02 |
| 0.539 | 1.369 E-02 |
| 0.567 | 1.440 E-02 |
| 0.628 | 1.595 E-02 |

## Stress

| KSI | MPa |
|---|---|
| 3 | 20.7 |
| 5 | 34.5 |
| 10 | 68.9 |
| 13 | 89.6 |
| 18 | 124.1 |
| 21 | 144.8 |
| 27 | 186.2 |
| 28 | 193.1 |
| 30 | 206.8 |
| 32 | 220.6 |
| 33 | 227.5 |
| 35 | 241.3 |
| 36 | 240.2 |
| 38 | 262.0 |
| 40 | 275.8 |
| 45 | 310.3 |
| 47 | 324.1 |
| 48 | 330.9 |
| 51 | 351.6 |
| 52 | 358.5 |
| 54 | 372.3 |
| 55 | 379.2 |
| 56 | 386.1 |
| 62 | 427.5 |
| 64 | 441.3 |
| 65 | 448.2 |
| 66 | 455.1 |
| 71 | 489.5 |
| 75 | 517.1 |
| 77 | 530.9 |
| 80 | 551.6 |
| 84 | 579.2 |

DISTRIBUTION LIST

Defense Documentation Center (12)
Cameron Station
Alexandria, VA 22314

Commander
US Army Armament Research and Development Command
ATTN: DRDAR-SC
DRDAR-SCP
DRDAR-SCM (10)
DRDAR-SCM-P (25)
DRDAR-TSS (5)
DRDAR-QA
DRCPM-CAWS
Dover, NJ 07801

Commander
US Army Materials and Mechanics Research Center
ATTN: DRXMR, Dr. E. Wright
DRXMR-PT
Watertown, MA 02172

Director
US Army Industrial Base Engineering Activity (2)
ATTN: DRXIB-MT
Rock Island, IL 61201

Weapon System Concept Team/CSL
ATTN: DRDAR-ACW
Aberdeen Proving Ground, MD 21010

Technical Library
ATTN: DRDAR-CLJ-L
Aberdeen Proving Ground, MD 21010

Technical Library
ATTN: DRDAR-TSB-S
Aberdeen Proving Ground, MD 21005

Benet Weapons Laboratory
Technical Library
ATTN: DRDAR-LCB-TL
Watervliet, NY 12189

Commander
U.S. Army Armament Materiel Readiness Command
ATTN: DRSAR-LEP-L
Rock Island, IL 61299

U.S. Army Materiel Systems Analysis Activity
ATTN: DRXSY-MP
Aberdeen Proving Ground, MD 21005

Project Manager
Production Base Modernization
ATTN: DRCPM-PBM-MA
Dover, NJ 07801